Comprehensive Analysis of Gly-Leu-Gly-Gly-Lys Peptide Dication Structures and Cation-Radical Dissociations Following Electron Transfer: From Electron Attachment to Backbone Cleavag...

ARTICLE *in* THE JOURNAL OF PHYSICAL CHEMISTRY A · DECEMBER 2013

Impact Factor: 2.69 · DOI: 10.1021/jp411100c · Source: PubMed

6 AUTHORS, INCLUDING:

Bo Peng
University of Washington Seattle
8 PUBLICATIONS **35** CITATIONS
SEE PROFILE

Aleš Marek
Academy of Sciences of the Czech Republic
23 PUBLICATIONS **91** CITATIONS
SEE PROFILE

Frantisek Turecek
University of Washington Seattle
237 PUBLICATIONS **9,698** CITATIONS
SEE PROFILE

THE JOURNAL OF PHYSICAL CHEMISTRY A

Article

pubs.acs.org/JPCA

Comprehensive Analysis of Gly-Leu-Gly-Gly-Lys Peptide Dication Structures and Cation-Radical Dissociations Following Electron Transfer: From Electron Attachment to Backbone Cleavage, Ion−Molecule Complexes, and Fragment Separation

Robert Pepin, Kenneth J. Laszlo, Bo Peng, Aleš Marek,[†] Matthew F. Bush, and František Tureček*

Department of Chemistry, Bagley Hall, Box 351700, University of Washington, Seattle, Washington 98195-1700, United States

Supporting Information

ABSTRACT: Experimental data from ion mobility measurements and electron transfer dissociation were combined with extensive computational analysis of ion structures and dissociation energetics for Gly-Leu-Gly-Gly-Lys cations and cation radicals. Experimental and computational collision cross sections of $(GLGGK + 2H)^{2+}$ ions pointed to a dominant folding motif that is represented in all low free-energy structures. The local folding motifs were preserved in several fragment ions produced by electron transfer dissociation. Gradient optimizations of $(GLGGK + 2H)^{+\bullet}$ cation-radicals revealed local energy minima corresponding to distonic zwitterionic structures as well as aminoketyl radicals. Both of these structural types can isomerize to low-energy tautomers that are protonated at the radical-containing amide group forming a new type of intermediates, $-C^{\bullet}O^{-}NH_2^{+}-$ and $-C^{\bullet}(OH)-NH_2^{+}-$, respectively. Extensive mapping with B3LYP, M06-2X, and MP2(frozen core) calculations of the potential energy surface of the ground doublet electronic state of $(GLGGK + 2H)^{+\bullet}$ provided transition-state and dissociation energies for backbone cleavages of the N−C_α and amide C−N bonds leading to ion−molecule complexes. The complexes can undergo facile prototropic migrations that are catalyzed by the Lys ammonium group and isomerize enolimine *c*-type fragments to the more stable amide tautomers. In contrast, interfragment hydrogen atom migrations in the complexes were found to have relatively high transition energies and did not compete with fragment separation. The extensive analysis of the intermediate and transition-state energies led to the conclusion that the observed dissociations cannot proceed competitively on the same potential energy surface. The reactive intermediates for the dissociations originate from distinct electronic states that are accessed by electron transfer.

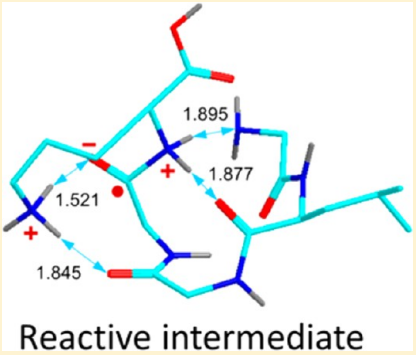

INTRODUCTION

Electron attachment to multiply charged peptide ions in the gas phase is a highly exothermic process that can be realized as electron−ion recombination or electron transfer from a charged or neutral donor. Electron−ion recombination forms the basis of electron-capture dissociation (ECD), a mass spectrometric technique that is chiefly performed on Fourier Transform ion cyclotron resonance instruments.[1] Electron transfer in a gas-phase anion−cation reaction is typically performed in ion traps using a plethora of gas-phase anions and is referred to as electron transfer dissociation (ETD).[2] Both processes, which are sometimes referred to under a common acronym ExD, result in extensive dissociation of peptide cation-radicals produced by electron attachment to the precursor, closed-shell, peptide ions. ExD have been of keen interest because of practical applications to peptide and protein sequencing,[3] as well as having been the target of fundamental studies of ion structures,[4−8] energetics,[6,9,10] electronic states,[6,11−13] and dissociation mechanisms, as recently reviewed.[14]

To achieve a comprehensive description of ExD of a peptide ion, one has to consider several consecutive and competitive processes that produce the fragment ions in the experimental ETD spectrum. This sequence begins with electron transfer from a molecular anion donor to the multiply charged peptide ion acceptor to form the charge-reduced peptide cation-radical in the ground or excited electronic states. The formation of electronic states is thought to be affected by the dipolar field surrounding the ion and superimposed on the Coulomb field of the peptide ion charge.[15−17] The ion dipole moment depends on the molecular geometry and charge distribution, which usually are unknown and have to be investigated. The ion geometry is determined by the nature and sequence of amino acid residues, protonation sites, and folding in the gas phase. The last two structural factors are often a priori unknown, contributing to the uncertainties in relating the precursor ion structure with dissociations upon ETD.

The peptide cation-radicals formed by electron transfer undergo competitive dissociations of N−H and N−C_α bonds producing first generation fragment ions and neutrals. These can undergo consecutive unimolecular dissociations to form

Received: November 11, 2013
Revised: December 11, 2013
Published: December 12, 2013

Scheme 1

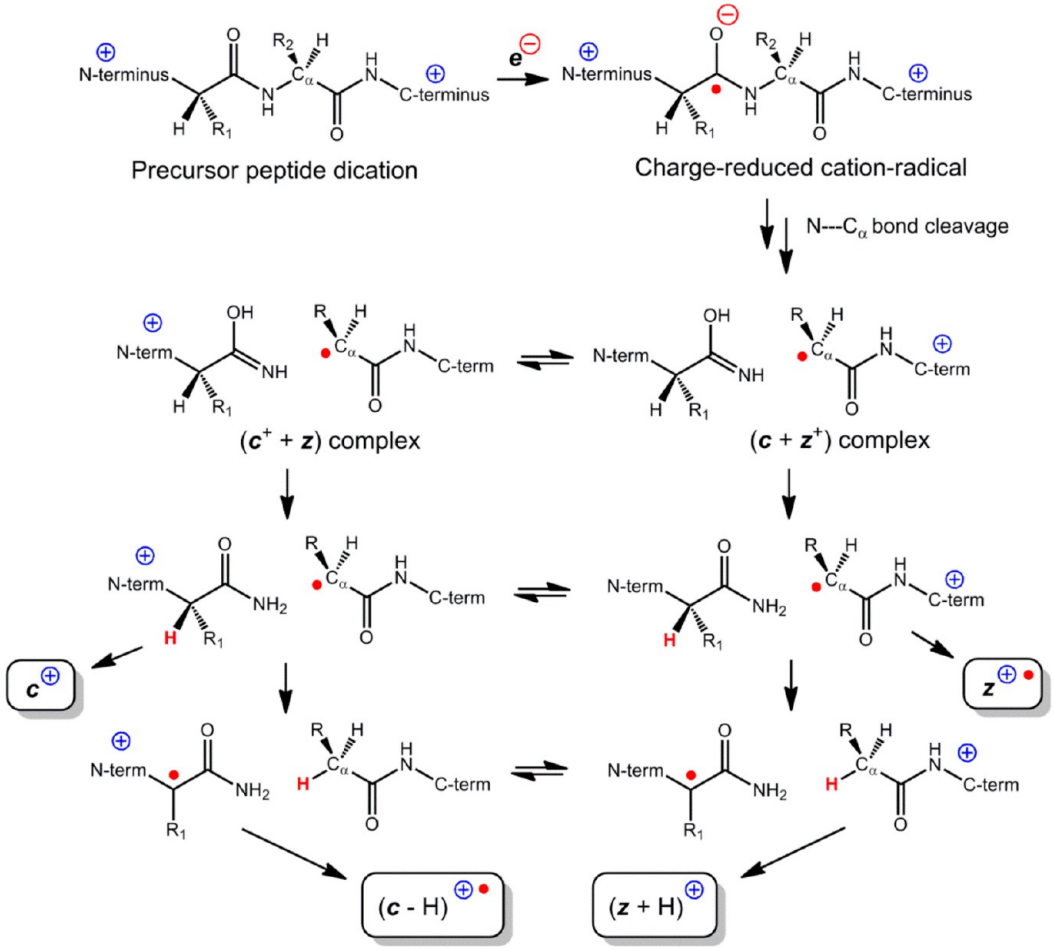

second generation fragments.[18−24] N−C_α bond dissociations produce noncovalent complexes of *N*-terminal (*c*) and *C*-terminal (*z*) fragments that can react by proton or hydrogen atom transfers before separation. These reactions are generically depicted in Scheme 1.

Selected aspects of ExD have been studied by experiment and theory for a variety of peptide ions. However, comprehensive, "from the cradle to the grave", investigations of ETD, starting with the precursor ion 3D structure and including electron transfer and dissociation energetics, multiple intermediates, and product ion structures have been confined to simple systems, such as dipeptide ions.[6,25] Thus far, no analysis has been attempted to *comprehensively* investigate the formation upon ETD of first and second generation fragment ions, characterize fragment ion−molecule complexes, and illustrate the energetics and kinetics of the pertinent processes within a larger peptide ion.

Here, we report a comprehensive study of electron attachment to doubly protonated Gly-Leu-Gly-Gly-Lys, $(GLGGK + 2H)^{2+}$. This model peptide was chosen to satisfy several criteria. First, this ion incorporates eleven protons in seven polar groups that are capable of hydrogen bonding to five carbonyl electron donors. This feature was presumed to give the gas-phase precursor dication sufficient flexibility for intramolecular hydrogen bonding to define its gas-phase conformation. Second, this peptide has only two basic amino groups that become the energetically favored protonation sites in the dication. This feature removes the ambiguity of the formation of tautomeric precursor ions. Finally, the $(GLGGK + 2H)^{2+}$ dication has five N−C_α bonds to be potentially cleaved upon electron transfer, thus allowing one to study several competitive reactions. We report several novel features describing the energies and electronic structure of the peptide cation radicals and transition states for their dissociations that shed light on the complex hydrogen and proton transfer reactions accompanying the backbone cleavages.

EXPERIMENTAL SECTION

Materials and Methods. The peptides, Gly-Leu-Gly-Gly-Lys (GLGGK), (Gly-2,2-d_2)-Leu-Gly-Gly-Lys (d_2-GLGGK), and Ala-Leu-Gly-Gly-Lys (ALGGK), were synthesized on the solid phase (Wang resin, Bachem Americas, Torrance, CA, and Chem-Impex Intl., Wood Dale, IL) using standard f-moc methods,[26] and their purity was checked by electrospray mass spectrometry. The fully D-labeled peptide ions, $(GLGGK\text{-}d_9 + 2D)^{2+}$, were generated by dissolving the peptide in 1:1 D_2O CH_3OD (99.5% D) that contained 0.5% CD_3COOD to achieve a 7−10 μM concentration and allowing the solution to stand for several hours, typically overnight, in a tightly capped vial. The peptide solution was infused with a syringe pump into an open electrospray source consisting of a pulled fused silica capillary as the ESI needle that was positioned 2 mm from the orifice of the source transfer capillary.[27] Simultaneously with electrospraying the D_2O/CH_3OD peptide solution, a stream of nitrogen that was saturated with D_2O vapor was blown over the

dx.doi.org/10.1021/jp411100c | J. Phys. Chem. A 2014, 118, 308−324

orifice and tip of the ESI needle from a 20-mm o.d. Pyrex tubing that was brought within 2 mm of the ESI tip.

Electron transfer dissociation (ETD) mass spectra were measured on a Thermo Electron Fisher linear quadrupole ion trap (LTQ-ETD) instrument equipped with an auxiliary chemical ionization ion source for the generation of fluoranthene anions as electron donors. Doubly charged peptide ions were produced from 1 to 5 μM solutions in 50:50:1 methanol−water-acetic acid in an open electrospray ion source. The ions were mass selected, stored in the linear ion trap and reacted with mass selected fluoranthene anions for 25, 50, 75, 100, 150, 200, and 300 ms. High resolution ETD mass spectra were measured on a Thermo Electron Fisher Orbitrap Velos ETD mass spectrometer with the resolving power set to 60 000 and on a Thermo Electron Fisher Orbitrap Elite ETD mass spectrometer at 120 000 resolution, using 200 ms ion−ion reaction times in both series of measurements.

Ion mobility measurements of $(GLGGK + 2H)^{2+}$ and its ETD fragments were measured using a modified Waters Synapt G2 HDMS (Waters Co., Manchester, U.K.).[28,29] For ETD experiments, nitrogen gas seeded with azulene vapor was passed through a needle positioned behind the first source orifice.[30] A potential was applied to the needle for 100 ms to generate a glow discharge. The resulting azulene radical anions were selected with the quadrupole and accumulated in the trap cell. Then, $(GLGGK + 2H)^{2+}$ ions generated from nano-electrospray ionization from a pulled borosilicate glass capillary were selected by the quadrupole and entered the trap cell to react with the stored anions for 1000 ms. Absolute mobilities (K) were measured using a 25.2 cm radio frequency confining drift cell containing 2.0 Torr of helium gas,[31,32] which replaced the traveling-wave ion mobility cell. Inside this cell, ions experience a constant time-average electric field; thus K can be determined directly from the measured drift times, pressure, and temperature. Most K values were determined from the slopes of a drift time versus reciprocal drift voltage plots ($r^2 > 0.998$) containing measurements at ∼10 drift voltages ranging from 104−353 V. Some values for low-intensity ions were determined by using a single drift time measurement and an estimate of the residence time of the ion between the exit of the ion mobility cell and the entrance of the mass analyzer (t_0). Collision cross sections were determined from K and the Mason−Schamp equation.[33]

Calculations. Conformational analysis was carried out using the ConformSearch software described previously.[34] Briefly, molecular dynamics trajectories were run with NAMD[35] and the CHARMM force field[36] at 8 temperatures using a replica exchange[37] scheme that generated 800 000 conformers of each peptide ion. The replica structures were sampled at regular intervals to extract 8000 structures that were fully optimized with PM6.[38] The optimized structures were sorted out into families sharing the same hydrogen bonding motifs and the families were compacted by sorting out duplicates. One hundred lowest-energy structures from the PM6 families were used to calculate B3LYP/6-31+G(d,p) single-point energies and the structures were resorted by energy. The 40 lowest-energy structures were then fully optimized with B3LYP[39,40] and M06-2X[41] calculations with the 6-31+G(d,p) basis set, duplicates were compacted, and the structures were characterized by frequency calculations as local energy minima. The harmonic frequencies were scaled by 0.963 and 0.954 for the B3LYP and M06-2X data, respectively, and used to obtain zero-point energy corrections, enthalpies, and entropies. The entropies were further corrected for contributions of low-frequency modes that were identified as hindered internal rotations.[42,43] Further energy ranking was based on energies obtained with B3LYP, M06-2X, and Møller−Plesset[44] (MP2, frozen core) single-point calculations using the larger 6-311++G(2d,p) basis set. Cation-radical structures were obtained by spin-unrestricted UB3LYP and UM06-2X/6-31+G(d,p) geometry optimizations and confirmed as local energy minima by harmonic frequency analysis. Transition-state structures were searched by stepwise potential energy mapping and confirmed by frequency calculations, showing one imaginary frequency. The connection of transition states to the reactants and intermediates was checked by intrinsic reaction coordinate analysis[45,46] of 10 forward and 10 reverse steps starting from the TS geometry. Single-point energies for cation-radicals were obtained by UB3LYP, UM06-2X, and UMP2(frozen core) calculations with the 6-311++G(2d,p) basis set. The DFT calculations showed spin expectation values $\langle S^2 \rangle$ of <0.76, indicating low contamination from quartet and higher spin states. The UMP2 energies showed $\langle S^2 \rangle$ = 0.76−0.81 for local energy minima and 0.76−0.97 for transition states. The spin contamination was corrected by the standard spin anihilation procedure[47,48] and the resulting energies are denoted as PMP2. These corrections resulted in $\langle S^2 \rangle$ < 0.752 and <0.76 for local minima and transition states, respectively, and the associated root-mean-square energy decreases were 2.3 and 5.0 millihartree (6.2 and 13.2 kJ mol^{-1}) for local minima and transition states, respectively. The B3LYP and spin-projected MP2 energies were averaged (B3-PMP2) to cancel small errors inherent to both approximations.[49,50] This empirical procedure has been shown to provide relative energies of improved accuracy for peptide ions and radicals.[6,34] Excited-state energies were calculated using time-dependent DFT theory[51] and the B3LYP and M06-2X hybrid functionals with the 6-311++G(2d,p) basis set. All electronic structure calculations were carried out with the Gaussian 09 suite of programs.[52] Atomic charge and spin densities were calculated with the natural population analysis (NPA) method.[53] Complete optimized structures (Cartesian standard orientations) as well as total and zero-point vibrational energies can be obtained from the corresponding author upon request.

Unimolecular rate constants were calculated for reactions occurring on the calculated B3-PMP2 and M06-2X potential energy surfaces that included zero-point vibrational energy corrections, using the Rice−Ramsperger−Kassel−Marcus (RRKM) theory[54] and the program of Zhu and Hase[55] that had been modified to deal with larger molecular systems with up to 1000 atoms, and recompiled to run under Windows XP[56] and Windows 7. The RRKM rate constants were obtained by direct count of quantum states at internal energies that were increased in 2 kJ mol^{-1} steps from the transition state up to 400 kJ mol^{-1} above the reactant. Rotations were treated adiabatically, and the calculated microscopic rate constants k(E,J,K) were then Boltzmann-averaged over the thermal distribution of rotational states at 298 K.

RESULTS

Electron Transfer Dissociations. The doubly charged $(GLGGK + 2H)^{2+}$ ions and their isotopologues underwent ion−ion reactions with fluoranthene anions that showed pseudo-first-order kinetics with apparent rate constants of 7.6−9.4 s^{-1} (Figure S1, Supporting Information). Electron transfer resulted in a nearly complete dissociation, so no

Table 1. Relative Intensities of Major Fragment Ions

	GLGGK		G(2,2-d_2)LGGK		d_{11}-GLGGK	
ion	m/z	rel intensity[a]	m/z	rel intensity[a]	m/z	rel intensity[a]
M + (H, D)	431.2612	24(0.9)[b]	433	24(0.5)[b]	441	9.1(0.4)
M + 2(H, D) − N(H, D)$_3$(z_5)	415.2425	8.7(0.4)	417	8.2(0.3)	423	10(0.7)
z_5 − C_3H_7	372.1877	4.9(0.1)	374	4.3(0.1)	380	4.5(0.3)
z_5 − C_4H_8	359.1799	14(0.4)	361	13(0.2)	367	14(0.9)
z_4	358.2211	1.2(0.04)	358	1.1(0.02)	365	1.2(0.1)
z_4 − C_3H_7	315.1663	3.7(0.1)	315	3.5(0.1)	322	3.5(0.2)
c_4	302.1823	11(0.2)	302	11(0.4)	310	11(0.8)
c_4 − H	301.1745	0.1(0.01)	301	0.5(0.01)		
y_3	261.1557	1.7(1.2)[c]	261	6.2(2.1)[c]	269	10.5(4.2)[c]
z_3 + H	246.1448	0.2(0.01)			252	0.3(0.3)
z_3	245.1370[c]	10(1)	245	11(1.4)	251	11(2.3)[c]
c_3	245.1608	1	247	0.8(0.03)	252	1(0.1)
z_2 + H	189.1233	1(0.03)	189	0.9(0.01)	194	1.2(0.1)
z_2	188.1155	2.1(0.8)	188	2.0(0.04)	193	2.1(0.2)
c_2	188.1393	<0.1	190	0.2		
y_1	147.1128	2.2(0.2)	147	2.3	153	1.6(0.2)
y_1 − H	146.1050	1.2(0.1)	146	1.5	152	1.3(0.2)
z_1 + H	132.1019	0.6[d]				
z_1	131.0941	0.09[d]				
total fragments		88(2)		80(1)		83(1)

[a]Percent relative to the sum of all ETD fragment ions. [b]Mean relative intensities and standard deviations from measurements at 50, 100, 200, and 300 ms ion−ion reaction times. [c]The z_3 and y_3 ion on intensities were time-dependent. [d]Extrapolated from first-order decay kinetics.

charge-reduced $(GLGGK + 2H)^{+\bullet}$ ions were detected in the spectra. Most of the fragment ion relative intensities showed flat dependence on the ion−ion interaction time over 50−300 ms, indicating that the dissociations were sufficiently fast to be complete at our shortest observation time. The fragment ion relative intensities are summarized in Table 1. A large fraction of ETD resulted in deprotonation or H atom loss, forming the m/z 431 ions from $(GLGGK + 2H)^{2+}$. This can be due to a peptide proton transfer to fluoranthene anion in an acid−base reaction, or electron transfer followed by hydrogen atom loss from the charge-reduced peptide cation-radical. These processes give rise to isobaric peptide ion products and cannot be readily distinguished in the spectra. The ETD mass spectrum of the $(d_9$-GLGGK+ 2D$)^{2+}$ ion, in which all OH and NH protons were exchanged for deuterium, showed a markedly decreased m/z 441 $(d_9$-GLGGK + D$)^+$ ion intensity of 9.1% compared to 24% $(GLGGK + H)^+$ formed from $(GLGGK + 2H)^{2+}$. This decrease can be attributed to isotope effects on both proton transfer and loss of H from the ammonium groups in the charge-reduced ion. In particular, loss of H from ammonium radicals has been reported to display large isotope effects.[57−61]

The majority (~60%) of ion fragments by ETD of $(GLGGK + 2H)^{2+}$ were formed by N−C_α bond dissociations. Cleavage of the N−C_α bond at the *N*-terminal Gly_1 comprised 27% of fragments formed by loss of ammonia (z_5 fragment ion) and consecutive leucine side-chain dissociations by loss of C_3H_7 and C_4H_8 from the z_5 ions. The assignment of the loss of ammonia ions as z_5 fragments was based on previous studies that used specific ^{15}N labeling in homologous Lys *C*-terminated ions.[62] It was also supported by the CID-MS^3 mass spectrum of the z_5 ion (Figure S2, Supporting Information) which showed radical-driven dissociations in the Leu and Lys residues, such as loss of C_3H_7 (43.0546 Da), C_4H_8 (56.0625 Da), C_3H_9N (59.0733 Da), and C_4H_9N (71.0734 Da) neutral radicals or molecules, which are typical of peptide *z*-type cation-radicals.[21−23]

Cleavage of the Leu_2 N−C_α bond gave rise to 4.9% of combined z_4 ions and their secondary (z_4 − C_3H_7) products. Dissociation at Gly_3 produced 11% of combined z_3, z_3 + H, and c_2 ions. Cleavage at Gly_4 was less effective, producing 3.5% of combined z_2, z_2 + H, and c_3 ions. Cleavage at Lys_5 formed 12% of combined c_4, c_4 − H, z_1, and z_1 + H ions. The N−C_α bond dissociation at Lys_5 involved proton transfer favoring the formation of the c_4 fragment ion over the complementary z_1 ion. Note that the z_3 and c_3 fragment ions at m/z 245 as well as the z_2 and c_2 fragment ions at m/z 188 are nominally isobaric and overlap in the low-resolution ETD mass spectra of $(GLGGK + 2H)^{2+}$. The z_3/c_3 overlap was unambiguously resolved in high resolution ETD mass spectra, which showed a 10:1 ratio of z_3 (m/z 245.1364) and c_3 (m/z 245.1603), favoring the z_3 ion. The z_2 and c_2 ions were of very low relative intensity in the high-resolution ETD mass spectra. These fragments were distinguished using mass shifts in the ETD mass spectra of isotopically labeled derivatives. For example, in the ETD mass spectra of the G(d_2)LGGK ion, the z_2 and z_3 ions did not contain the heavy Gly_1 residue and their m/z and were not shifted (Table 1).

The ETD mass spectrum of the completely D-exchanged (d_9-GLGGK + 2D$)^{2+}$ ion showed z_5, z_4, z_3, z_2, and c_4 backbone fragments with mass shifts that were appropriate for the expected number of exchangeable protons in these ions (Table 1). The respective fragment relative intensities, combined with those of their secondary dissociation products, were 28, 4.8, 12, 3.3, and 11%. These figures were very similar to those from ETD of $(GLGGK + 2H)^{2+}$ and (G(d_2)LGGK + 2H$)^{2+}$ ions and indicated very small isotope effects on the backbone dissociations.

The time dependence of the fragment ion relative intensities was monitored in the range 25−300 ms, as shown for (d_9-GLGGK + 2D$)^{2+}$ (Figure S3, Supporting Information). Most fragment ions showed a flat time profile after 50 ms, indicating that the rate constants for their formation were greater than

dx.doi.org/10.1021/jp411100c | J. Phys. Chem. A 2014, 118, 308−324

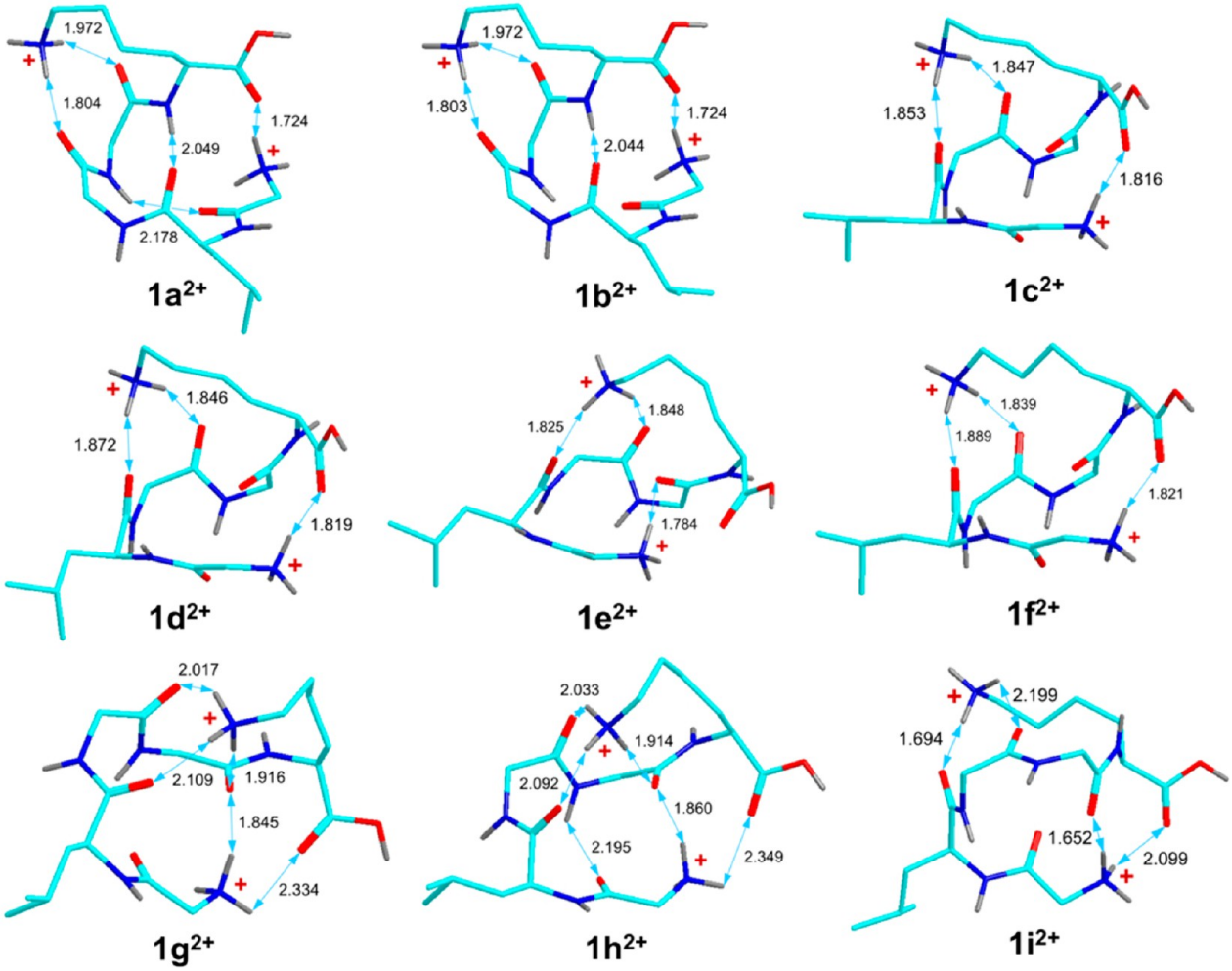

Figure 1. M06-2X/6-31+G(d,p) optimized structures of lowest-energy $(GLGGK + 2H)^{2+}$ ions. The atom color coding is as follows: turquoise green = C, blue = N, red = O, silver gray = H. Only exchangeable OH and NH hydrogen atoms are shown. Hydrogen bonds are indicated by blue double-headed arrows and the interatomic distances are in Ångstrøms.

100 s^{-1}. In contrast, the z_3 and y_3 ions showed time-dependent intensity profiles. The z_3 ion relative intensity increased with time with an apparent rate constant estimated at 12−15 s^{-1}. This is much lower than the rate constants estimated for the other backbone cleavages, indicating that the dissociation leading to the z_3 ion did not proceed competitively from the same pool of charge-reduced precursor ions. The relative intensity of the y_3 ions exponentially decreased at longer ion−ion reaction times. This is likely due to the depletion by electron transfer of the precursor dications by the pseudo-first-order reaction with the fluoranthene anion.[8] The y_3 ions are readily formed by collisional excitation of precursor dications.

In summary, the GLGGK ions demonstrated multiple backbone cleavages, side-chain losses, and proton and hydrogen atom transfers in their ETD mass spectra, which are reactions that are typical of the majority of charge-reduced peptide ions.[14]

Precursor and Fragment Ion Structures. A conformational search of $(GLGGK + 2H)^{2+}$ ion structures identified several low-energy conformers. The lowest-energy conformers $\mathbf{1a}^{2+}$−$\mathbf{1i}^{2+}$ are shown in Figure 1, and their energies are summarized in Table 2. Somewhat unexpectedly for such a small peptide ion, the calculated equilibrium population of conformers was dominated by conformers $\mathbf{1a}^{2+}$ and $\mathbf{1b}^{2+}$ (Figure 1). These showed nearly identical hydrogen bonding patterns where the charged lysine ammonium group formed hydrogen bonds to the Gly_3 and Gly_4 amide carbonyls, and the charged *N*-terminal ammonium group formed a hydrogen bond

Table 2. Relative Energies of $(GLGGK + 2H)^{2+}$ Ions

	relative energy[a]			dipole moment (D)	
ion	B3LYP[b]	M06-2X[c]	MP2[b]	B3LYP	M06-2X
$\mathbf{1a}^{2+}$	0.0	0.0	0.0	5.3	5.7
$\mathbf{1b}^{2+}$	4.8 (4.6)[d]	3.2 (1.4)[e]	4.4 (4.2)[d]	5.0	5.6
$\mathbf{1c}^{2+}$	17 (8.4)	18 (11)	24 (15)	5.0	3.9
$\mathbf{1d}^{2+}$	16 (12)	20 (18)	24 (23)	4.3	3.2
$\mathbf{1e}^{2+}$	18 (16)	20 (18)	21 (19)	4.2	4.4
$\mathbf{1f}^{2+}$	25 (25)	20 (20)	21 (24)	4.7	4.1
$\mathbf{1g}^{2+}$	27 (28)	19 (20)	23 (24)	6.3	5.6
$\mathbf{1h}^{2+}$	28 (31)	17 (20)	21 (24)	7.3	6.8
$\mathbf{1i}^{2+}$	15 (12)	25 (19)	20 (18)	3.9	4.0

[a]In kJ mol^{-1}. [b]Including B3LYP/6-31+G(d,p) zero-point energy corrections. [c]Including M06-2X/6-31+G(d,p) zero-point energy corrections. [d]The values in parentheses are 298 K relative free energies that include B3LYP/6-31+G(d,p) enthalpies, entropies, and hindered rotor corrections. [e]The values in parentheses are 298 K relative free energies that include M06-2X/6-31+G(d,p) enthalpies, entropies, and hindered rotor corrections.

dx.doi.org/10.1021/jp411100c | J. Phys. Chem. A 2014, 118, 308−324

to the carboxyl group. This spatial arrangement allowed for efficient internal solvation of both charged groups while balancing the attractive ion-dipole interactions with Coulomb repulsion of the charged groups. Structures $\mathbf{1a}^{2+}$ and $\mathbf{1b}^{2+}$ showed two other hydrogen bonds between the neutral groups, one involving the leucine amide carbonyl and the Gly_4 amide proton, and the other involving the Gly_1 amide carbonyl and the Gly_3 amide proton. The latter hydrogen bond was substantially tighter in the M06-2X optimized structure of $\mathbf{1a}^{2+}$ than in the B3LYP optimized structure, as illustrated by the respective O---H bond lengths, which were 2.178 and 2.546 Å (Figure 1). Conformer $\mathbf{1b}^{2+}$ differs from $\mathbf{1a}^{2+}$ in the rotation of the Leu side-chain isopropyl group.

Other conformers were calculated to have notably higher enthalpies and 298 K free energies than $\mathbf{1a}^{2+}$ and $\mathbf{1b}^{2+}$. For example, conformers $\mathbf{1c}^{2+}$ and $\mathbf{1d}^{2+}$, which are Leu side-chain rotamers, have ionic hydrogen bonding patterns similar to that in $\mathbf{1a}^{2+}$ and $\mathbf{1b}^{2+}$ but lack one of the neutral amide hydrogen bonds (Figure 1). Conformers $\mathbf{1c}^{2+}$ and $\mathbf{1d}^{2+}$ had somewhat higher entropies than did $\mathbf{1a}^{2+}$ and $\mathbf{1b}^{2+}$. The calculated free energies indicated that a 298 K equilibrium should be dominated by $\mathbf{1a}^{2+}$ (64−84%) and $\mathbf{1b}^{2+}$ (36−16%) with small populations of $\mathbf{1c}^{2+}$(0.2−2.8%) and $\mathbf{1d}^{2+}$ (0.01−0.7%) being present. The population ranges reflect differences in the relative free energies calculated by B3LYP, M06-2X, and MP2 (Table 2). The entropy effect can increase the populations of $\mathbf{1c}^{2+}$ and $\mathbf{1d}^{2+}$ if the ions were sampled at higher temperatures or excited by collisional activation. Higher energy structures $\mathbf{1e}^{2+}$−$\mathbf{1i}^{2+}$ listed in Table 2 and several others were calculated to have negligible populations at equilibrium. Fully optimized structures were also obtained for ETD fragment cation-radicals z_1, z_2, z_3, and z_4, and even-electron ions z_4 + H, and c_4. The M06-2X optimized fragment ion structures are shown in Figure S4 (Supporting Information).

Collisional Cross Sections. The optimized geometries and Mulliken atomic charges were used to calculate collisional cross sections (Ω) for the precursor ion conformers and fragment ions and compare them to the experimental data from ion mobility measurements. The experimental Ω of $(GLGGK + 2H)^{2+}$ was measured as 136 ± 3 Å^2. The experimental and calculated Ω are summarized in Table 3.[63,64] It may be noted that calculations that used atomic charge densities from Mulliken and natural population analysis[53] gave collisional cross sections within 0.3% of each other and were considered equivalent. The data showed a narrow range of theoretical collisional cross sections, Ω = 132−140 Å^2 for $\mathbf{1a}^{2+}$, $\mathbf{1b}^{2+}$, $\mathbf{1c}^{2+}$, $\mathbf{1e}^{2+}$, and $\mathbf{1i}^{2+}$. In particular, the Ω of these conformers that were based on M06-2X geometries and charge densities were nearly identical (Table 3). This result followed from the very similar ionic hydrogen bonding patterns in the low-energy conformers where the *N*-terminal and lysine side-chain ammonium groups adopted an antiparallel orientation that ensured energetically most favorable internal solvation of both charged groups. Although the experimental and theoretical collisional cross sections did not allow us to assign a particular conformer to the gas−phase dications, they clearly pointed to the group of conformers with the hydrogen bonding pattern represented in all lowest free-energy structures. Another feature of ion structures $\mathbf{1a}^{2+}$−$\mathbf{1i}^{2+}$ was that they had a narrow range of dipole moments, μ = 3.9−5.3 D (Table 3), again consistent with the very similar alignments of the charged and polar groups in these ions.

Collisional cross sections were also measured and calculated for ETD fragment ions c_4, z_4, z_3, and y_1 (Table 3). The calculated cross sections showed a trend depending on the optimized geometry and method used to convert the geometry to the Ω values. The closest agreement was obtained for data from trajectory method calculations that were based on M06-2X optimized structures, which showed a 4.1% maximum and 2.9% root-mean square deviation from the experimental cross sections. The B3LYP optimized structures also gave a close agreement with experiment (4.8% maximum, 2.9% rmsd) when treated with the trajectory method. These results showed that the calculated structures were representative of the fragment ion geometries even though these were obtained without an exhaustive conformational search. The close match of the calculated and experimental structures indicated that the fragments preserved the local folding motifs from the precursor ions.[34] This gave us some confidence that also the calculated fragment ion energies could be used for realistic approximations of the dissociation energetics.

Cation-Radical Structures and Energies. The geometries of the low-energy dication conformers $\mathbf{1a}^{2+}$, $\mathbf{1c}^{2+}$, and $\mathbf{1i}^{2+}$ were used as initial structures in a search for cation-radicals formed by electron attachment. Several local energy minima were found for cation-radicals as summarized in Figure 2. The relationship of the cation-radical to its precursor dication is denoted by an arrow, as in $1a^{2+} \rightarrow \mathbf{1a}^{+\bullet}$.

Electron attachment to the lowest-energy conformer $\mathbf{1a}^{2+}$ was calculated to be associated with vertical recombination energies of RE_{vert} = 4.62−4.93 eV by MP2 and M06-2X, respectively. The adiabatic recombination energy was RE_a = 5.61 and 5.97 eV by MP2 and M06-2X, respectively. The difference in the vertical and adiabatic recombination energies was due to the substantial geometry relaxation upon gradient optimization of the cation-radical structures. The pertinent local energy minimum obtained by both B3LYP and M06-2X corresponded to a *zwitterionic structure* ($\mathbf{1a}^{+\bullet}$, Figure 2) consisting of a Gly_1 amide anion-radical and the positively charged *N*-terminal and Lys ammonium groups. The zwitterionic nature of cation radical $\mathbf{1a}^{+\bullet}$ followed from the electron density distribution, which showed that 91% of unpaired spin density was localized in the reduced Gly_1 amide group, with a major part being at the puckered amide carbon atom. The Gly_1 amide oxygen and nitrogen carried large

Table 3. Collisional Cross Sections (Å^2)[a] for $(GLGGK + 2H)^{2+}$ Conformers

	B3LYP		M06-2X		exp.
structure	PA[b]	TM[c]	PA[b]	TM[c]	mean ± std dev
$\mathbf{1a}^{2+}$	138	140	135	136	136 ± 3
$\mathbf{1b}^{2+}$	137	139	134	136	
$\mathbf{1c}^{2+}$	135	137	132	133	
$\mathbf{1e}^{2+}$	136	138	134	134	
$\mathbf{1i}^{2+}$	135	137	132	135	
c_4^+	109	107	107	104	103 ± 0.5
$z_4^{+\bullet}$	125	122	119	117	121 ± 0.1
c_3^+	99	94	98	92	89[d,e]
$z_3^{+\bullet}$	94	89	93	88	89[d,e] ± 0.9
y_1^+	72	66	71	65	66 ± 0.5

[a]In helium. [b]From projection approximation calculations.[63] [c]From optimized trajectory method calculations.[64] [d]A 10:1 mixture of nominally isobaric $z_3^{+\bullet}$ and c_3^+ fragments ions. [e]Determined using one drift-time measurement and an estimate of t_0.

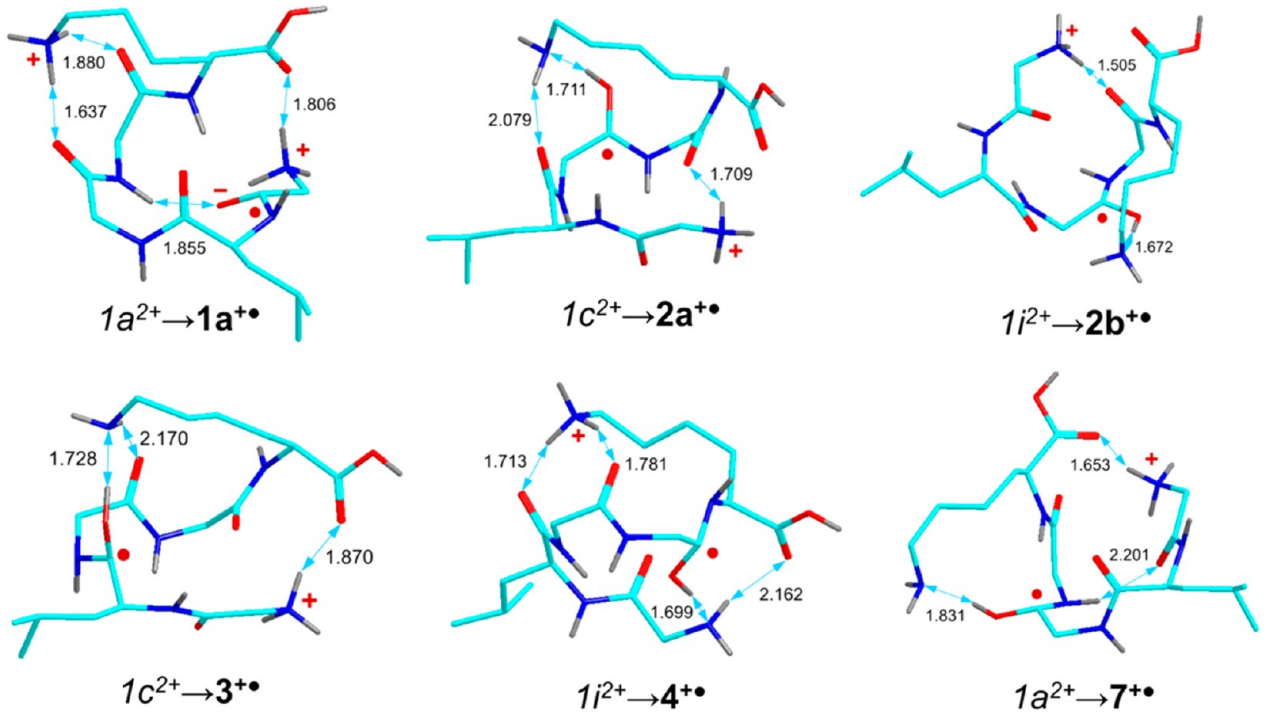

Figure 2. M06-2X/6-31+G(d,p) optimized structures of $(GLGGK + 2H)^+$ cation-radicals. The atom and hydrogen bond color coding is as Figure 1.

Table 4. Relative Energies of Cation-Radicals

	relative energy[a,b]				relative energy[a,b]		
ion/reaction	B3LYP	M06-2X	PMP2	ion/reaction	B3LYP	M06-2X	PMP2
1a$^{+\bullet}$	0	0	0	**4**$^{+\bullet}$ → **TS10**	24	*e*	42
2a$^{+\bullet}$	3	18	17	**12**$^{+\bullet}$ → **TS11**	37	32	40
2b$^{+\bullet}$	−4	15	10	**21**$^{+\bullet}$ → **TS12**	4	6	13
3$^{+\bullet}$	14	19	26	**12**$^{+\bullet}$ → **TS13**	76	69	58
4$^{+\bullet}$	−18	−2	−2	**24**$^{+\bullet}$ → **TS14**	54	67	49
5$^{+\bullet}$	29	18	23	**14**$^{+\bullet}$ → **TS16**	58	105	88
6$^{+\bullet}$	−32	−38	−27	**1a**$^{+\bullet}$ → $z_5^{+\bullet}$ + NH_3	−111	−74	−88
7$^{+\bullet}$	11	22	23	**1a**$^{+\bullet}$ → $z_4^{+\bullet}$ + c_1(enolimine)	−25	40	46
8$^{+\bullet}$	12	*c*	19	**1a**$^{+\bullet}$ → $z_4^{+\bullet}$ + c_1(amide)	−95	−25	−23
9$^{+\bullet}$	−19	−26	−34	**1a**$^{+\bullet}$ → $z_1^{+\bullet}$ + c_4	−33	41	50
Ala-**1a**$^{+\bullet}$ → Ala-**9**$^{+\bullet}$	−4	−7	−15	**1a**$^{+\bullet}$ → $z_1^{\bullet}$ + c_4^+(amide)	−47	31	35
10$^{+\bullet}$	*d*	−29	*d*	**1a**$^{+\bullet}$ → y_1^+ + $b_4^{\bullet}$	74	152	148
11$^{+\bullet}$	−138	−115	−129	**9**$^{+\bullet}$ → **11**$^{+\bullet}$	32	64	62
12$^{+\bullet}$	−91	−64	−60	**7**$^{+\bullet}$ → **15**$^{+\bullet}$	−15	0.7	14
13$^{+\bullet}$	−149	−109	−108	**2a**$^{+\bullet}$ → **16**$^{+\bullet}$	45	*e*	63
14$^{+\bullet}$	13	38	28	**2a**$^{+\bullet}$ → $z_3^{+\bullet}$ + c_2(amide)	−52	6	6
1a$^{+\bullet}$→ **TS1**	23	20	17	**2b**$^{+\bullet}$ → **17**$^{+\bullet}$	−22	6	−2
1a$^{+\bullet}$ → **TS2**	−2	−4	−3	**4**$^{+\bullet}$ → **18**$^{+\bullet}$	20	*e*	46
1a$^{+\bullet}$ → **TS3**	0.2	11	7	**4**$^{+\bullet}$ → **19**$^{+\bullet}$	0.5	*e*	17
6$^{+\bullet}$ → **TS3**	32	49	34	**20**$^{+\bullet}$	−95	−60	−60
1a$^{+\bullet}$ → **TS4**	7	21	22	**21**$^{+\bullet}$	−118	−64	−60
6$^{+\bullet}$ → **TS4**	39	59	49	**21**$^{+\bullet}$ → **22**$^{+\bullet}$	−54	−43	−45
1a$^{+\bullet}$ → **TS5**	22	46	40	**1a**$^{+\bullet}$ → **22**$^{+\bullet}$	−179	−105	−113
9$^{+\bullet}$ → **TS5**	40	73	74	**12**$^{+\bullet}$ → **22**$^{+\bullet}$	−82	−42	−47
9$^{+\bullet}$ → **TS6**	18	37	41	**12**$^{+\bullet}$ → **23**$^{+\bullet}$	−47	−42	−45
1a$^{+\bullet}$ → **TS7**	57	31	74	**1a**$^{+\bullet}$ → **24**$^{+\bullet}$	−179	−105	−113
2a$^{+\bullet}$ → **TS8**	50	*e*	59	**12**$^{+\bullet}$ → **24**$^{+\bullet}$	−53	−50	−45
2b$^{+\bullet}$ → **TS9**	41	*e*	62	**14**$^{+\bullet}$ → **25**$^{+\bullet}$	−102	−61	−64

[a]In kJ mol^{-1}. [b]Including zero-point energy corrections and referring to 0 K. [c]M06-2X gradient optimizations collapsed to structure **10**$^{+\bullet}$. [d]B3LYP gradient optimizations collapsed to structure **9**$^{+\bullet}$. [e]These calculations did not lead to transition states.

dx.doi.org/10.1021/jp411100c | J. Phys. Chem. A 2014, 118, 308−324

Scheme 2

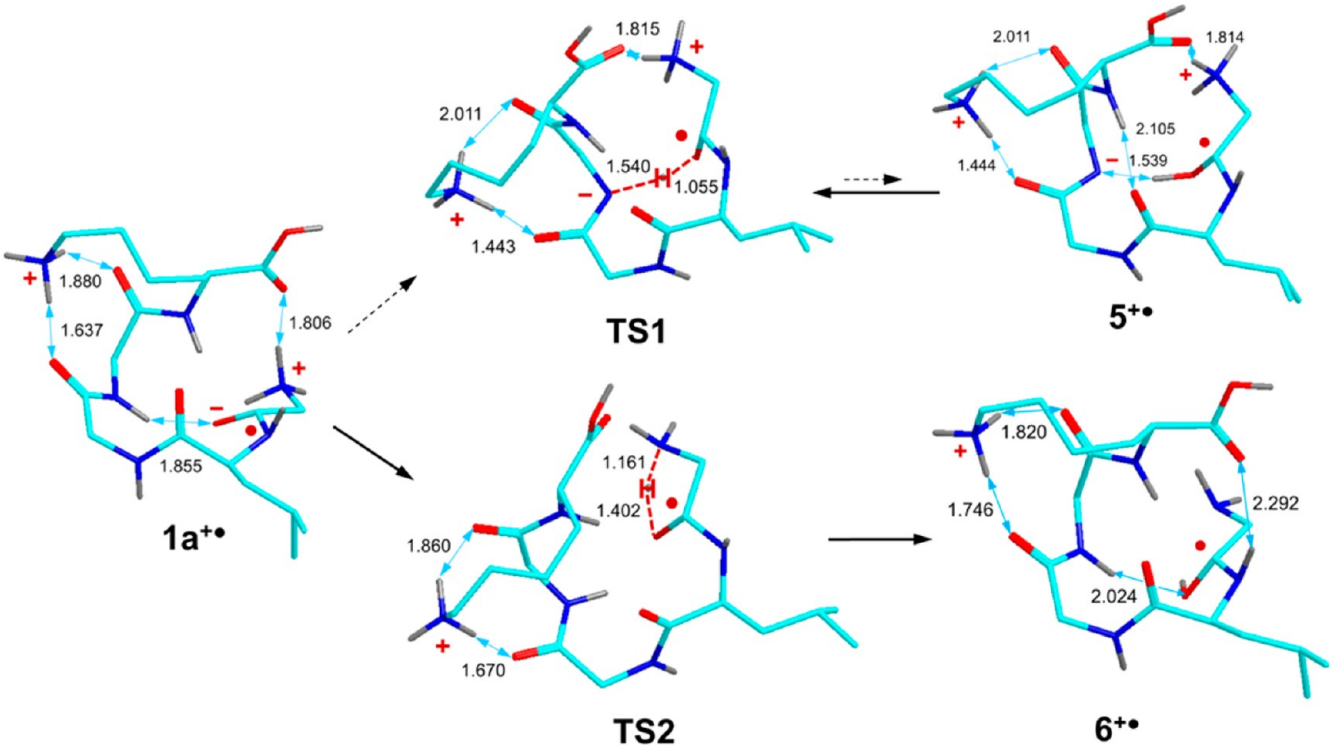

negative charges, −0.91 and −0.70, respectively. The pertinent Gly_1 amide C−O bond was elongated to 1.32−1.33 Å, whereas the other amide C═O bonds had standard lengths of 1.23−1.25 Å. Analogous zwitterions have been reported for other peptide cation-radicals[65] and appear to represent a rather common structural type produced by electron attachment to peptide ions.[14]

The formation of $\mathbf{1a}^{+\bullet}$ can be followed by analyzing the electronic states of the cation-radical ($\mathbf{1a}^{+\bullet}$(vert)) produced by vertical electron attachment to $\mathbf{1a}^{2+}$. Note that $\mathbf{1a}^{+\bullet}$(vert) is a construct representing a *landing point* on the potential energy surface, not a stationary point for any of the electronic states in $\mathbf{1a}^{+\bullet}$. The TD-DFT wave functions for the 15 lowest electronic states (**A** through **O**) in $\mathbf{1a}^{+\bullet}$(vert) showed electron delocalization among the *N*-terminal and lysine ammonium 3s Rydberg-like orbitals (**X** and **A** states, respectively), and combinations of amide and carboxyl π^* orbitals (**B**, **C**, and higher excited states, Figure S5, Supporting Information). Vibrational relaxation in the **X** state of $\mathbf{1a}^{+\bullet}$(vert) led to the **X** state of $\mathbf{1a}^{+\bullet}$ with the associated ∼1 eV lowering of potential energy. The first excited state (**A**) of $\mathbf{1a}^{+\bullet}$ showed electron promotion to a combination of carboxyl and Gly_4 amide π^* orbitals (Figure S5, Supporting Information). It is noteworthy that the **X** → **A** excitation energy in $\mathbf{1a}^{+\bullet}$ (1.68 and 2.68 by B3LYP and M06-2X, respectively) was greater than the **X** → **O** excitation energy in $\mathbf{1a}^{+\bullet}$ (vert), indicating that the **A** state with the relaxed geometry was energetically inaccessible from the low excited states in $\mathbf{1a}^{+\bullet}$(vert).

We searched for other zwitterionic structures produced by relaxation of an excited state of $\mathbf{1a}^{+\bullet}$(vert) in which the electron entered a different amide group. However, upon gradient optimization these constructs collapsed to $\mathbf{1a}^{+\bullet}$ or underwent proton migrations forming tautomeric cation-radicals $\mathbf{5}^{+\bullet}$−$\mathbf{10}^{+\bullet}$. The relative energies of these peptide cation radicals obtained at three levels of theory are summarized in Table 4, the M06-2X energies are discussed in the text.

In the search for further types of cation-radicals we also investigated electron attachment to dications $\mathbf{1c}^{2+}$ and $\mathbf{1i}^{2+}$. These were selected because their H-bonding patterns slightly differed from that in $\mathbf{1a}^{2+}$, a feature that could affect the electronic states accessed by electron transfer. Specifically, the *N*-terminal ammonium in $\mathbf{1c}^{2+}$ and $\mathbf{1i}^{2+}$ was internally solvated by the Gly_4 amide carbonyl, and the Lys ammonium had strong H-bonds to the Leu and Gly_3 amide carbonyls. Electron attachment to $\mathbf{1c}^{2+}$ followed by gradient optimization resulted in a spontaneous migration of a Lys ammonium proton to the Gly_3 amide, forming the Gly_3 aminoketyl radical $\mathbf{2a}^{+\bullet}$ (Figure 2) which was at a slightly higher energy than $\mathbf{1a}^{+\bullet}$. This process could be altered by artificially puckering the Leu amide carbonyl in $\mathbf{1c}^{2+}$, in which case electron attachment and geometry relaxation resulted in Lys proton migration to the Leu amide group and formation of the Leu aminoketyl radical $\mathbf{3}^{+\bullet}$. The latter cation-radical was 19 kJ mol^{-1} less stable than $\mathbf{1a}^{+\bullet}$. Electron attachment to $\mathbf{1i}^{2+}$, followed by geometry relaxation, formed the Gly_4 aminoketyl radical $\mathbf{4}^{+\bullet}$, which was 10 kJ mol^{-1} more stable than $\mathbf{1a}^{+\bullet}$. An attempt to generate a Leu amide radical from $\mathbf{1i}^{2+}$ resulted in a collapse to another conformer of the Gly_3 aminoketyl radical ($\mathbf{2b}^{+\bullet}$).

Proton Migrations in Cation-Radicals. Cation-radical $\mathbf{1a}^{+\bullet}$ that was spontaneously produced as a local energy minimum upon gradient optimization was further investigated regarding tautomer-forming proton migrations. Migration of a proton from the neutral Gly_3 amide group onto the negatively charged Gly_1 amide oxygen in $\mathbf{1a}^{+\bullet}$ formed cation-radical $\mathbf{5}^{+\bullet}$ (Scheme 2). This was a zwitterionic aminoketyl-imidate tautomer in which the spin density was localized in the neutral Gly_1 aminoketyl group, whereas the deprotonated Gly_3 amide group carried a negative charge. Tautomer $\mathbf{5}^{+\bullet}$ was 18 kJ mol^{-1} less stable than $\mathbf{1a}^{+\bullet}$ into which it could isomerize by a reverse

dx.doi.org/10.1021/jp411100c | J. Phys. Chem. A 2014, 118, 308−324

proton migration after crossing a miniscule energy barrier in the transition state (**TS1**, E_{TS1} = 2 kJ mol^{-1} relative to **5**$^{+\bullet}$).

Migration of a proton from the charged *N*-terminal ammonium group onto the Gly_1 amide oxygen in **1a**$^{+\bullet}$ (Scheme 2) formed cation-radical **6**$^{+\bullet}$ (−38 kJ mol^{-1} relative to **1a**$^{+\bullet}$). Ion **6**$^{+\bullet}$ was a proper aminoketyl radical[10] that was characterized by the unpaired electron density and pyramidization at the Gly_1 C(OH)NH atom. The exothermic **1a**$^{+\bullet}$ → **6**$^{+\bullet}$ proton migration required overcoming a very small potential energy barrier in the pertinent transition state (**TS2**) that vanished upon inclusion of zero-point vibrational energies to give *E*(**TS2**) = −2.4 kJ mol^{-1} relative to **1a**$^{+\bullet}$. Hence, **1a**$^{+\bullet}$ can be considered to be dynamically unstable with respect to this exothermic isomerization. Dynamic instability has been reported for other zwitterionic peptide cation radicals.[14,65]

Electron attachment to the Gly_3 amide in **1a**$^{2+}$ did not form an amide anion-radical as a local energy minimum but triggered a spontaneous migration of a Lys ammonium proton, forming aminoketyl radical **7**$^{+\bullet}$ (Figure 2) which was another conformer of **2a**$^{+\bullet}$. This spontaneous proton migration indicated that the intermediate Gly_3 amide anion radical was a stronger base than lysine, consistent with the previously proposed concept of superbasicity of amide π^* states.[11] Radical **7**$^{+\bullet}$ was 22 kJ mol^{-1} less stable than zwitterion **1a**$^{+\bullet}$ (Table 3).

An interesting result was obtained by attaching an electron to the Gly_4 amide group in **1a**$^{+\bullet}$. The intermediate anion-radical can undergo spontaneous isomerization by Lys proton migration, forming an aminoketyl radical (**8**$^{+\bullet}$, 15 kJ mol^{-1} relative to **1a**$^{+\bullet}$ according to B3-PMP2), which is a conformer of **4**$^{+\bullet}$ (Figure 2). However, a competing exothermic isomerization by migration of an *N*-terminal ammonium proton to the Gly_4 amide *nitrogen* in the anion-radical proceeded to form the amide-*N*-protonated cation-radical **9**$^{+\bullet}$ (−26 kJ mol^{-1} relative to **1a**$^{+\bullet}$). Structure **9**$^{+\bullet}$ (Scheme 3) was unprecedented in both its electronic properties and as a potential intermediate for competitive dissociations of the amide C−N and N−C_α bonds. The electron distribution in **9**$^{+\bullet}$ clearly indicated it was a Gly_4 amide anion radical where 92% of unpaired electron density was localized in the Gly_4 C−O group. This electron distribution was obtained by NPA analysis of both B3LYP and M06-2X electron densities and did not appear to be an artifact of the particular DFT method. The Gly_4 amide C$^\bullet$O$^-$ and protonated NH_2 groups in **9**$^{+\bullet}$ respectively carried a −0.4 and +0.22 charge, attesting to the dipolar character of the CO−NH_2 moiety. Cation-radical **9**$^{+\bullet}$ can undergo a further isomerization by migration of a Lys ammonium proton forming ion **10**$^{+\bullet}$ (−29 kJ mol^{-1} relative to **1a**$^{+\bullet}$), which is an N-protonated Gly_4 aminoketyl radical. The very similar energies of **9**$^{+\bullet}$ and **10**$^{+\bullet}$ indicated that these structures could readily interconvert by proton migration.

The existence of structures **9**$^{+\bullet}$ and **10**$^{+\bullet}$ as local energy minima is contingent upon similar topical basicities of the *N*-terminal Gly_1 amino group, which is protonated in **1a**$^{+\bullet}$, and the nitrogen atom in the reduced Gly_4 amide group, which is protonated in **9**$^{+\bullet}$ and **10**$^{+\bullet}$. This interpretation was substantiated by calculations of the relative energies of homologous species, Ala_1-**1a**$^{+\bullet}$ and Ala_1-**9**$^{+\bullet}$ derived from ALGGK (Figure S6, Supporting Information). Replacing the Gly_1 residue with the more basic Ala_1 caused the ΔH_0(Ala-**1a**$^{+\bullet}$→Ala-**9**$^{+\bullet}$) energy difference decrease to −7 kJ mol^{-1} compared to a much larger value of −26 kJ mol^{-1} for the energy difference for **1a**$^{+\bullet}$ → **9**$^{+\bullet}$.

Finally, attempts to attach an electron to the Leu_2 amide group resulted in a collapse to structure **1a**$^{+\bullet}$. Note that the Leu_2 amide group did not form hydrogen bonds to the *N*-terminal and Lys ammonium groups in the precursor ion **1a**$^{2+}$ and, at a 4.7−5.9 Å O···NH_3 distance, it was relatively remote from the charged groups. Presumably, an anion-radical intermediate produced by electron attachment to Leu_2 amide in **1a**$^{2+}$ was not efficiently stabilized by Coulomb effects of the charged ammonium groups and collapsed to lower-energy structures.

Backbone Dissociations. Cation-radicals **1a**$^{+\bullet}$−**10**$^{+\bullet}$ were used as initial structures for studying backbone dissociations and loss of ammonia. These are the main dissociations experimentally observed in ETD of (GLGGK + 2H)$^{2+}$ ions (Table 1). The loss of ammonia was considered to involve the *N*-terminal ammonium group,[62] and therefore the dissociation was started from structure **1a**$^{+\bullet}$. Upon stretching the *N*-terminal H_3N−C bond and rotating the NH_3 group about the CH_2—CO bond, the system reached a low-energy transition state (**TS3**) at 4 kJ mol^{-1} above **1a**$^{+\bullet}$ (Scheme 4). The departing ammonia molecule can briefly stay engaged in a low-energy ion−molecule complex (**11**$^{+\bullet}$) with the $z_5^{+\bullet}$ fragment ion, which was −115 kJ mol^{-1} relative to **1a**$^{+\bullet}$. Note, however, that the configuration in complex **11**$^{+\bullet}$ was such that the ammonia molecule was held by two hydrogen bonds to the incipient $z_5^{+\bullet}$ fragment ion, and so it had to reorient from the initial configuration after N−C_α bond cleavage. Because the potential energy surface along the forward trajectory from **TS3** was steeply repulsive, it was possible that the departing NH_3 molecule gained substantial kinetic energy[25] and missed the potential energy minimum of complex **11**$^{+\bullet}$. A complete dissociation to separated z_5 and NH_3 fragments was also substantially exothermic (−74 kJ mol^{-1} relative to **1a**$^{+\bullet}$).

The loss of ammonia competed with the isomerization of **1a**$^{+\bullet}$ to aminoketyl radical **6**$^{+\bullet}$ (Scheme 2). The branching ratio for these reactions, which presumably occur on the same potential energy surface, can depend on the dynamics of the system, as previously reported for (AR + 2H)$^{+\bullet}$.[25] Alter-

Scheme 3

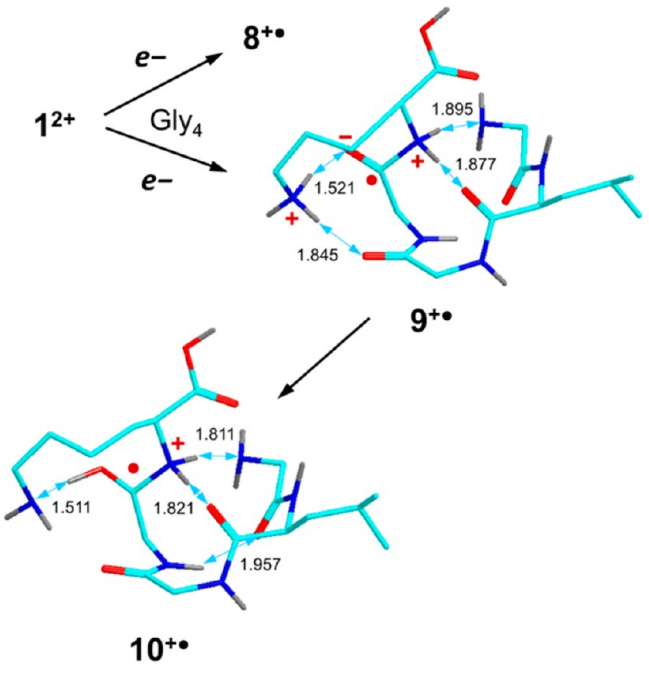

dx.doi.org/10.1021/jp411100c | J. Phys. Chem. A 2014, 118, 308−324

Scheme 4

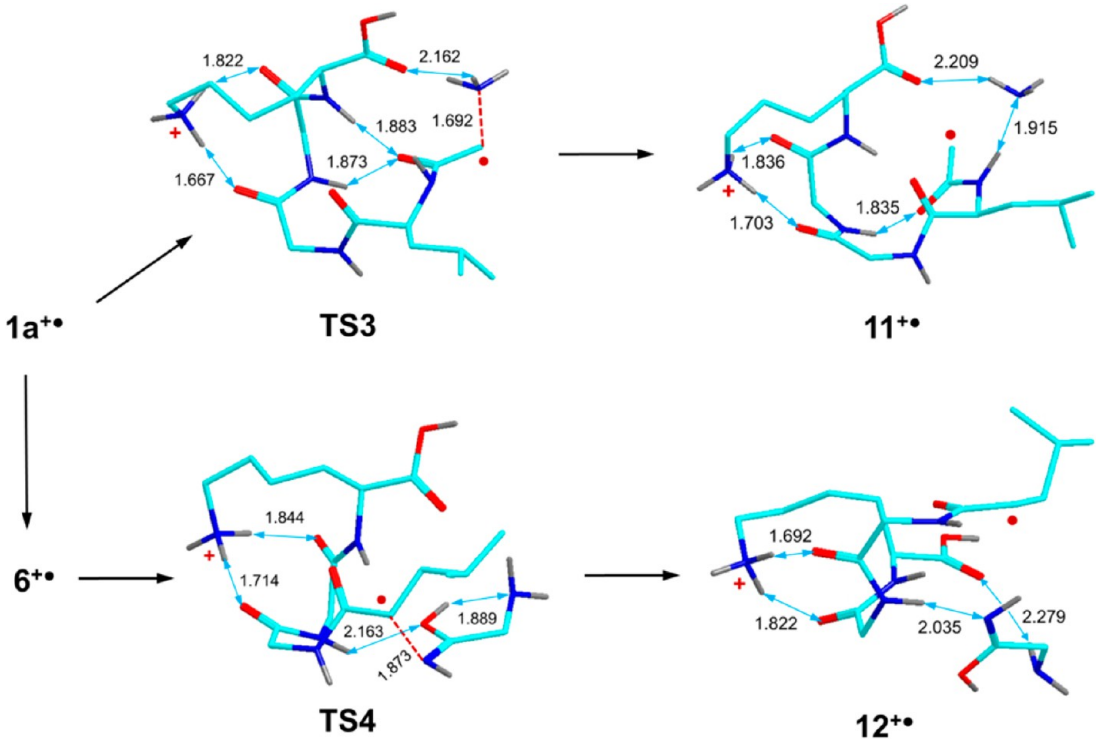

natively, the reaction branching could occur from structure $\mathbf{6}^{+\bullet}$ and be governed by the vibrational-state densities in the pertinent TS. The TS energy for the cleavage of the Gly_1-Leu amide N−C_α bond in $\mathbf{6}^{+\bullet}$ (**TS4**) was calculated to be 21 kJ mol^{-1} relative to $\mathbf{1a}^{+\bullet}$, which was slightly higher than the **TS3** energy. The dissociation exothermically proceeded to an ion−molecule complex ($\mathbf{12}^{+\bullet}$) consisting of an anti−anti enolimine conformer of the neutral $\boldsymbol{c}_1$ fragment and the $\boldsymbol{z}_4^{+\bullet}$ ion. Complex $\mathbf{12}^{+\bullet}$ had a potential energy that was −64 kJ mol^{-1} relative to $\mathbf{1a}^{+\bullet}$. A complete dissociation of $\mathbf{1a}^{+\bullet}$ to the $\boldsymbol{z}_4^{+\bullet}$ ion and neutral $\boldsymbol{c}_1$ fragments was 40 kJ mol^{-1} endothermic when forming $\boldsymbol{c}_1$ as an enolimine tautomer, or 25 kJ mol^{-1} exothermic when forming $\boldsymbol{c}_1$ as the more stable glycine amide molecule.

The question of the dynamic versus statistical control of $\mathbf{1a}^{+\bullet}$ dissociations was addressed by obtaining the pertinent RRKM unimolecular rate constants for $\mathbf{6}^{+\bullet}$ competitively dissociating via **TS3** (k_3) and **TS4** (k_4). The rate constants were calculated on the M06-2X and B3-PMP2 potential energy surfaces for a 50−410 kJ mol^{-1} range of internal energies (Figure 3). The rate constants showed a rapid increase with the ion internal energy (E) to reach $k > 100$ s^{-1} at $E > 100$ kJ mol^{-1}, which was consistent with >99% dissociation of the charge-reduced ions on the experimental time scale (50−300 ms). The experimental branching ratio for these reactions was expressed as a ratio of the pertinent fragment ion relative intensities, $[z_4]/[M + 2H - NH_3] = 0.18$. These relative intensities were compounded to include the secondary fragments by loss of C_3H_7 and C_4H_8. To compare the RRKM branching ratios with the experimental value, the calculated rate constants have to be convoluted with an internal energy distribution function, $P(E)$, according to eq 1, where $(k_3 + k_4)t \gg 1$.

$$\frac{k_4}{k_3} = \frac{\int_{E_{04}}^{E} P(E)\frac{k_4(E)}{k_3(E)+k_4(E)}(1 - e^{-(k_3+k_4)t})\,dE}{\int_{E_{03}}^{E} P(E)\frac{k_3(E)}{k_3(E)+k_4(E)}(1 - e^{-(k_3+k_4)t})\,dE} \cong \frac{\int_{E_{04}}^{E} P(E)\frac{k_4(E)}{k_3(E)+k_4(E)}\,dE}{\int_{E_{03}}^{E} P(E)\frac{k_3(E)}{k_3(E)+k_4(E)}\,dE} \quad (1)$$

Factoring out the time dependence in eq 1 was justified by the fact that the experimental $[z_4]/[M + 2H - NH_3]$ ratio stayed flat over the range of experimental reaction times, indicating $(k_3 + k_4)t \gg 1$. The data indicated that the RRKM rate constants were in qualitative agreement with experiment. The branching ratios for the Gly-Leu N−C_α bond cleavage and loss of ammonia were $k_4/k_3 < 1$ and increased with internal energy when based on both the M06-2X and B3-PMP2 transition-state energies. However, the B3-PMP2 calculations underestimated the k_4/k_3 ratio by a factor of 3 over the entire range of internal energies (Figure 3a). The M06-2X calculations showed a crossover of the k_4 and k_3 curves at ∼190 kJ mol^{-1} (Figure 3b) whereas the experimental branching ratio was matched at a low internal energy of 125 kJ mol^{-1}. The Figure 3a,b data and further analysis indicated that the theoretical branching ratios were very sensitive to the quality of the calculated potential energy surface, in particular the TS energies. For example, adjusting the relative TS energies by 2 kJ mol^{-1} resulted in k_4/k_3 ratios that matched the experimental value over a range of internal energies. One can conclude that the loss of ammonia and Gly-Leu N−C_α bond cleavage can proceed as competitive reactions from populations of reactants with randomized internal energy. However, in spite of this qualitative agreement, the calculated TS energies were not accurate enough to extract the pertinent $P(E)$ function from eq

dx.doi.org/10.1021/jp411100c | J. Phys. Chem. A 2014, 118, 308−324

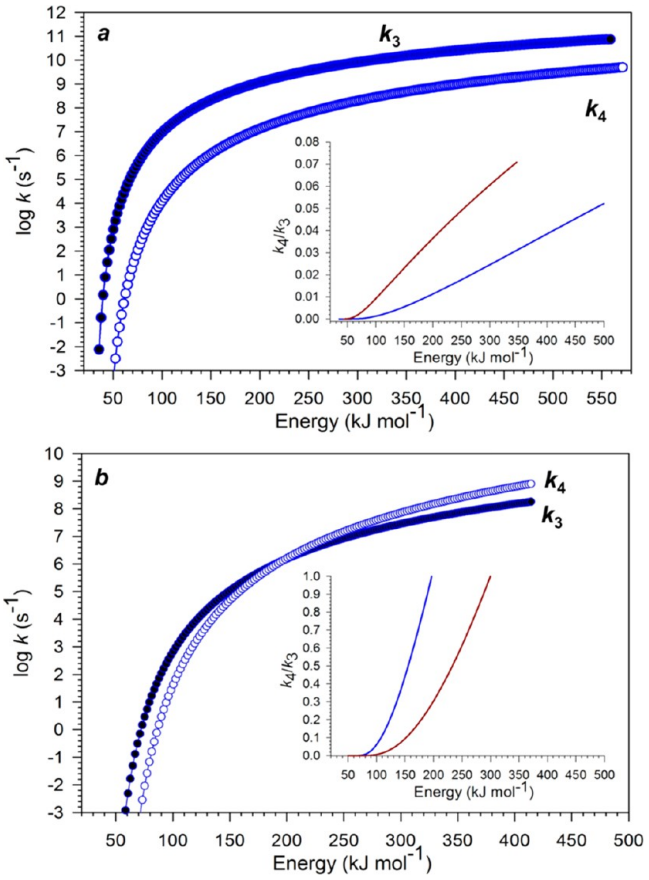

Figure 3. RRKM rate constants for the competing loss of ammonia (k_3, full circles) and N−C_α bond cleavage (k_4, open circles) obtained at (a) combined B3LYP and PMP2 and (b) M06-2X potential energy surfaces. Insets show the k_4/k_3 ratios at calculated TS energies (blue curves) and at those that were adjusted by 2 kJ mol^{-1} (brown curves).

1 and address the question of internal energy distribution upon ETD.

Structures $\mathbf{9}^{+\bullet}$ and $\mathbf{10}^{+\bullet}$ represented potential reactants for the cleavages of the N−C_α bond between the Gly_4 and Lys residues forming the z_1 and c_4 fragments (Scheme 5). The pertinent TS was found (**TS5**) that connected cation-radical $\mathbf{9}^{+\bullet}$ with complex $\mathbf{13}^{+\bullet}$ consisting of ${z_1}^{+\bullet}$ and c_4 fragments. The complex $\mathbf{13}^{+\bullet}$ energy was −109 kJ mol^{-1} relative to $\mathbf{1a}^{+\bullet}$. Interestingly, potential energy mapping along the N−C_α coordinate that started from $\mathbf{8}^{+\bullet}$ and $\mathbf{10}^{+\bullet}$ also converged to **TS5** and involved spontaneous migration of the aminoketyl OH proton to the Lys amino group when the N−C_α bond was stretched to d(N−C_α) > 1.75 Å. The **TS5** energy relative to $\mathbf{9}^{+\bullet}$ (73 kJ mol^{-1}) was higher than for **TS4** relative to aminoketyl radical $\mathbf{6}^{+\bullet}$ (59 kJ mol^{-1}). This difference was not important for the branching ratio of the pertinent N−C_α bond cleavages, because ions $\mathbf{6}^{+\bullet}$ and $\mathbf{9}^{+\bullet}$ were not interconvertible and thus the dissociation pathways through **TS3** and **TS5** were independent. The continuing dissociation of complex $\mathbf{13}^{+\bullet}$ depended on the formation of the complementary $({z_1}^{+\bullet} + c_4)$ or $(z_1^{\bullet} + {c_4}^{+})$ fragments differing in the position of the charging proton. The $\mathbf{1a}^{+\bullet} \rightarrow {z_1}^{+\bullet} + c_4$ pathway was 41 kJ mol^{-1} endothermic for the formation of the c_4 amide tautomer. The complementary $\mathbf{1a}^{+\bullet} \rightarrow z_1^{\bullet} + {c_4}^{+}$ pathway was 31 kJ mol^{-1} endothermic for the formation of ${c_4}^{+}$ as an *N*-terminus protonated GLGG amide. This energy difference reflects the higher proton affinity of GLGG amide (PA = 979 kJ mol^{-1} at 0 K) than the Lys z_1 radical (PA = 968 kJ mol^{-1} at 0 K). We also note that the *N*-terminus protonated GLGG amide was substantially more stable than its backbone-protonated tautomers and likely represented a low-energy structure.

A competing pathway was found to involve cleavage of the amide C−N bond in $\mathbf{9}^{+\bullet}$ (Scheme 5). This pathway proceeded through **TS6** whose energy was 37 kJ mol^{-1} relative to $\mathbf{9}^{+\bullet}$ to reach another complex ($\mathbf{14}^{+\bullet}$) of the incipient ${y_1}^{+}$ ion and $b_4^{\bullet}$ radical fragments. The lower energy of **TS6** relative to **TS5** indicated a faster dissociation to y_1 and b_4 radical fragments. However, complex $\mathbf{14}^{+\bullet}$ was at a 64 kJ mol^{-1} higher energy than $\mathbf{9}^{+\bullet}$, indicating that the $\mathbf{9}^{+\bullet} \rightarrow$ **TS6** $\rightarrow \mathbf{14}^{+\bullet}$ reaction was reversible. A further dissociation of $\mathbf{14}^{+\bullet}$ to the ${y_1}^{+}$ ion and $b_4^{\bullet}$ radical fragments was 106 kJ mol^{-1} endothermic. Part of this high energy may be due to an unfavorable conformation of the neutral b_4 radical fragment for which we could not perform exhaustive conformational analysis to locate the global energy minimum. Nevertheless, the data indicated that the flux through the $\mathbf{9}^{+\bullet} \rightarrow$ **TS6** $\rightarrow \mathbf{14}^{+\bullet} \rightarrow {y_1}^{+} + b_4^{\bullet}$ pathway was hampered by the high energies of the intermediates and products. Note that in the ETD mass spectrum the combined $(z_1^{\bullet} + c_4)^{+}$ fragments appear at 3.5-fold greater relative abundance than $(y_1 + b_4)^{+}$, which is in qualitative agreement with the calculated energetics.

Cation-radical $\mathbf{7}^{+\bullet}$, which is a Gly_3 aminoketyl intermediate, was considered as a reactant for cleavage of the Gly_3—Gly_4 N−C_α bond, leading to $(z_2^{\bullet} + c_3)^{+}$ fragments (Scheme 6). A TS for this dissociation (**TS7**) was found at an energy that was 31 kJ mol^{-1} above $\mathbf{1a}^{+\bullet}$. This dissociation led to complex $\mathbf{15}^{+\bullet}$ of incipient $(z_2^{\bullet} + c_3)^{+}$ fragments that was nearly isoenergetic with $\mathbf{7}^{+\bullet}$. The reaction coordinate leading to**TS7** showed some interesting properties. Elongation of the Gly_3—Gly_4 N−C_α bond in $\mathbf{7}^{+\bullet}$ was accompanied by proton transfers that were described slightly differently by B3LYP and M06-2X. The B3LYP **TS7** showed the breaking N−C_α bond at 1.818 Å while maintaining the enolimine configuration of the Gly_3 group. Simultaneously, the *N*-terminal ammonium group was on the verge of transferring a proton to the Gly_4 oxygen. These features were further pronounced in the M06-2X **TS7**, which showed the breaking N−C_α bond at a longer distance of 2.078 Å (Scheme 6). Simultaneously, the *N*-terminal proton completely moved to the Gly_4 oxygen whereas the Gly_3 enolimine proton was shared with the Lys amine group. Further progression along the reaction coordinate led to complex $\mathbf{15}^{+\bullet}$ which had a standard enolimine configuration in the incipient neutral c_3 fragment, whereas the ${z_2}^{+\bullet}$ fragment was an enol cation-radical having a neutral amino group in the Lys side chain. This configuration was not preserved in an isolated ${z_2}^{+\bullet}$ fragment ion which underwent an exothermic migration of the enol proton onto the Lys amine group, forming a standard C_α radical distonic structure. The intricate proton migrations accompanying the cleavage of the Gly_3—Gly_4 N−C_α bond were further illustrated in a stepwise fashion by intrinsic reaction coordinate analysis in the forward and reverse direction starting from **TS7**.

Enol Dissociation Pathways. Aminoketyl radical intermediates can undergo N−C_α bond cleavages on the C- or N-terminal sides of the aminoketyl group.[66,67] Cleavage on the *C*-terminal side forms the enolimine c and radical z fragments, as described above. Cleavage on the N-terminal side forms a (c − H) amidyl radical and an enol tautomer of the $(z + H)^{+}$ ion that must exchange a proton or a hydrogen atom to give rise to the c and z fragments.[14,66] We investigated enol dissociation

dx.doi.org/10.1021/jp411100c | *J. Phys. Chem. A* 2014, 118, 308−324

Scheme 5

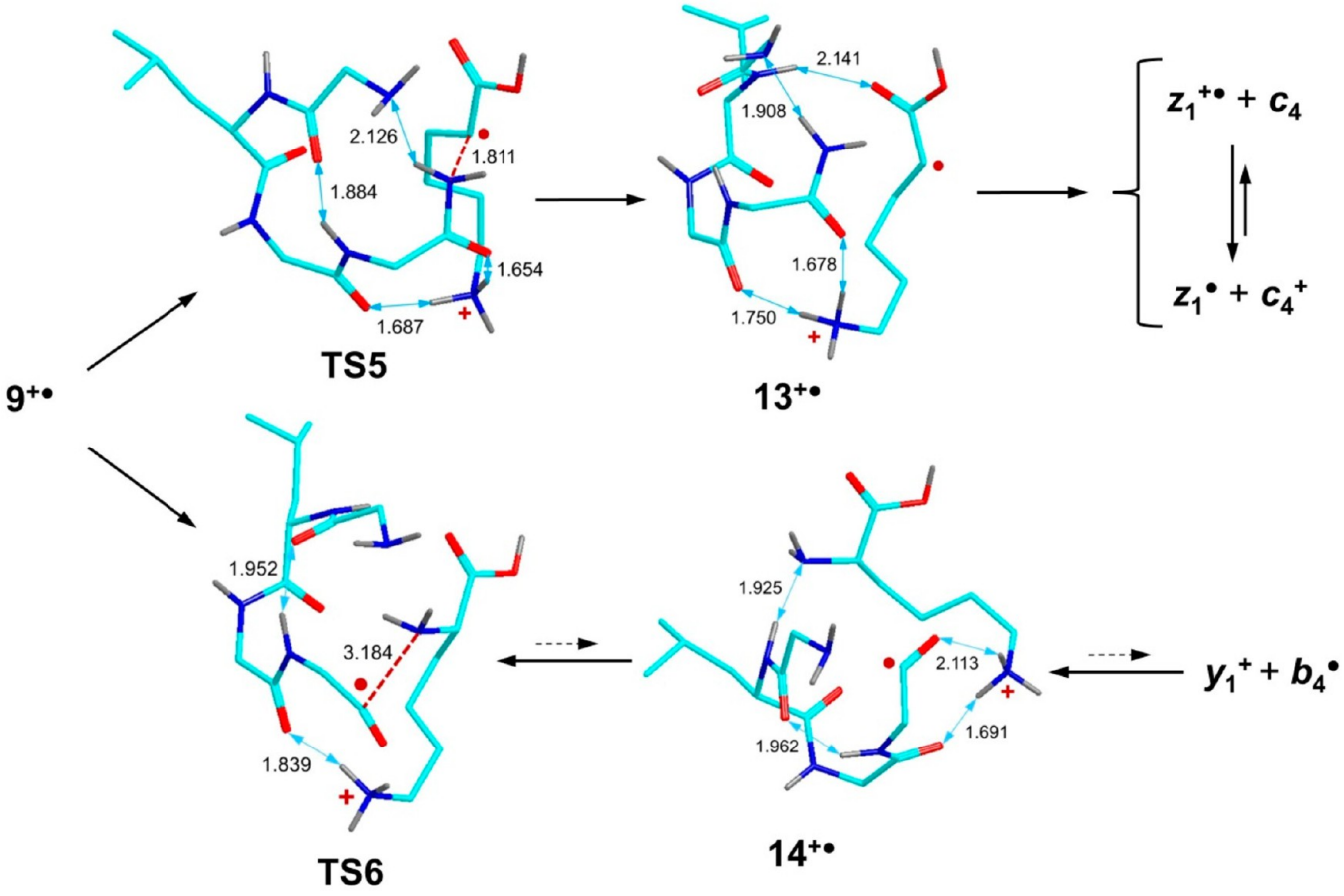

Scheme 6

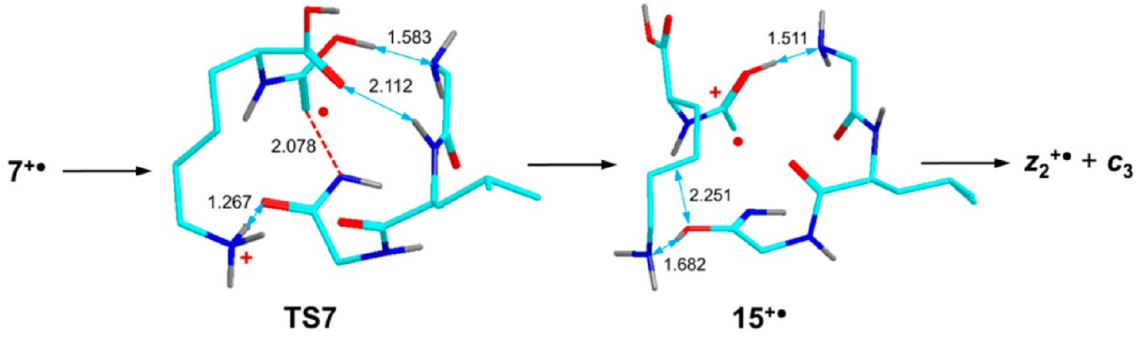

pathways starting from Gly_3 aminoketyl radicals $\mathbf{2a}^{+\bullet}$, $\mathbf{2b}^{+\bullet}$, and their Gly_4 tautomer $\mathbf{4}^{+\bullet}$. Ions $\mathbf{2a}^{+\bullet}$ and $\mathbf{2b}^{+\bullet}$ had similar energies but differed in the internal solvation of the aminoketyl group and the incipient Leu (c − H) fragment. The enol dissociation pathway starting from $\mathbf{2a}^{+\bullet}$ was investigated by a B3LYP search that led to **TS8** (50−59 kJ mol^{-1} relative to $\mathbf{2a}^{+\bullet}$, Table 4) and continued to a high-energy complex ($\mathbf{16}^{+\bullet}$) of the $(c_3 - H)^{+\bullet}$ amidyl cation radical and a neutral z_2 enol (Scheme S1, Supporting Information). However, this complex was not a local energy minimum on the M06-2X potential energy surface and collapsed back to $\mathbf{2a}^{+\bullet}$ upon gradient optimization. The enol pathway starting with $\mathbf{2b}^{+\bullet}$ converged to a very different TS (**TS9**, 41−62 kJ mol^{-1} relative to $\mathbf{2b}^{+\bullet}$). This showed an early N−C_α bond dissociation at 1.770 Å and was accompanied by a proton migration from the Gly_3 aminoketyl OH onto the Lys ε-amino group, showing **TS9** as a distinct zwitterionic structure. The resulting $c_2^+ + z_3^\bullet$ complex ($\mathbf{17}^{+\bullet}$) was close in energy to $\mathbf{2b}^{+\bullet}$ (Table 4). Again, reaction coordinate mapping and TS search with M06-2X did not produce a TS9-like transition state but resulted in a local energy minimum of a conformer of $\mathbf{2b}^{+\bullet}$.

Dissociation of the Gly_3-Gly_4 enol N−C_α bond in $\mathbf{4}^{+\bullet}$ proceeded through a low energy TS (**TS10**, 24−42 kJ mol^{-1} relative to $\mathbf{4}^{+\bullet}$, Table 4) leading to another complex ($\mathbf{18}^{+\bullet}$, Scheme S2, Supporting Information). The latter developed a very tight hydrogen bond between the amidyl oxygen and the Lys ammonium. Complex **18** can undergo a very facile and exothermic reverse formation of the N−C_α bond leading back to $\mathbf{4}^{+\bullet}$, which occurred spontaneously in geometry optimization with M06-2X. Alternatively, complex $\mathbf{18}^{+\bullet}$ can be stabilized by a

dx.doi.org/10.1021/jp411100c | J. Phys. Chem. A 2014, 118, 308−324

Scheme 7

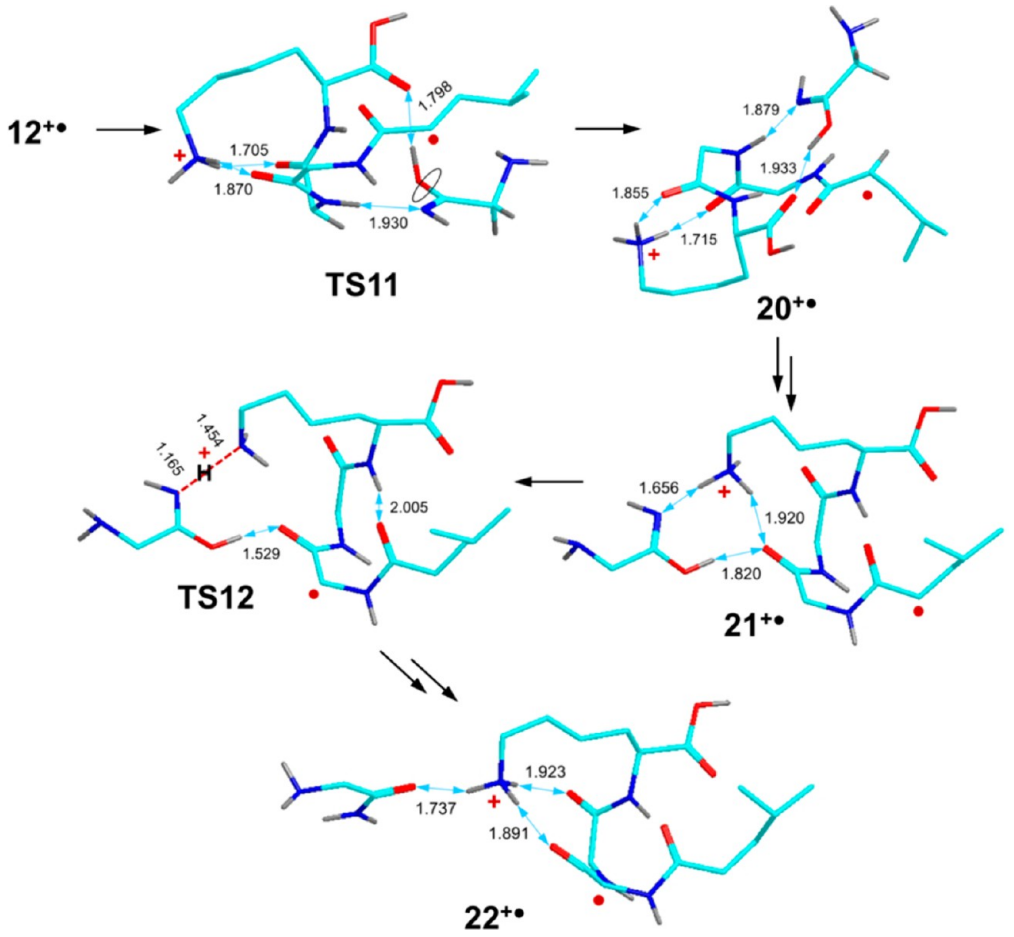

double proton transfer forming a new complex (**19**) of the incipient enolimine c_3^+ ion and a neutral $z_2^\bullet$ radical. Note that complex $\mathbf{19}^{+\bullet}$ is slightly less stable than $\mathbf{4}^{+\bullet}$ and can revert to it through **TS10** rather than continuing along the pathway for the highly endothermic separation of the c_3^+ and $z_2^\bullet$ fragments. This is consistent with the inefficient formation of c_3^+ ions in the ETD spectrum (Table 1). Overall, the N−C_α bond dissociations on the enol side of the aminoketyl radicals showed comparable TS energies as did the conventional dissociations on the amide side.[67] However, the intermediate $(c - H)^\bullet + (z + H)^+$ complexes $\mathbf{16}^{+\bullet}$ and $\mathbf{18}^{+\bullet}$ in the enol pathways containing *c*-fragment amide enol groups were substantially less stable than the $(c + z)^{+\bullet}$ complexes in the standard dissociation pathways.

Proton and Hydrogen Atom Transfer in Fragment Ion−Molecule Complexes. The ETD spectra of $(GLGGK + 2H)^{2+}$ showed that backbone cleavages of the Gly-Gly and Gly-Lys N−C_α bonds involved hydrogen atom transfers forming the corresponding $(z_2 + H)^+$ and $(z_1 + H)^+$ fragment ions (Table 1). In contrast, cleavage between Leu-Gly residues did not result in a hydrogen transfer forming $(z_4 + H)^+$ ions. Furthermore, the energy analysis indicated that the complementary *c* fragments, both neutrals and ions, were substantially more stable in the form of amide tautomers rather than enolimines. This raised the possibility of hidden exothermic rearrangements occurring in the course of the dissociations and resulting in lower-energy products. Proton and hydrogen atom transfers were investigated with complex $\mathbf{12}^{+\bullet}$, which is the first intermediate on the pathway leading to the observed $[z_4^{+\bullet} + c_1]$ and putative $[(z_4 + H)^+ + (c_1 - H)^\bullet]$ dissociation products. The c_1 neutral fragment in complex $\mathbf{12}^{+\bullet}$ has an anti−anti enolimine configuration that is unfavorable for an enolimine → amide isomerization by proton transfer. Rotation of the enolimine OH group in $\mathbf{12}^{+\bullet}$ through **TS11** formed a syn−anti conformer $\mathbf{20}^{+\bullet}$ that was nearly isoenergetic with $\mathbf{12}^{+\bullet}$ (Scheme 7). The **TS11** energy was 32 kJ mol^{-1} relative to $\mathbf{12}^{+\bullet}$ and substantially below the dissociation threshold to $[z_4^{+\bullet} + c_1]$. Complex $\mathbf{20}^{+\bullet}$ can undergo a cascade of conformational changes in which the c_1 fragment migrates about the refolding $z_4^{+\bullet}$ fragment to reach another complex ($\mathbf{21}^{+\bullet}$). The latter is nearly isoenergetic with $\mathbf{20}^{+\bullet}$ and has the Lys ammonium group coordinated to the c_1 enolimine moiety where it can facilitate prototropic enolimine−amide isomerization. This can readily proceed by Lys proton migration through **TS12** (at 6 kJ mol^{-1} relative to $\mathbf{21}^{+\bullet}$) followed by OH proton migration back to the Lys amine, forming the very stable c_1 amide complex $\mathbf{22}^{+\bullet}$ at −42 kJ mol^{-1} relative to $\mathbf{12}^{+\bullet}$ and −105 kJ mol^{-1} relative to $\mathbf{1a}^{+\bullet}$. Dissociation of complex $\mathbf{22}^{+\bullet}$ to the c_1 amide and $z_4^{+\bullet}$ ion was 80 kJ mol^{-1} endothermic.

Isomerizations proceeding by H atom migration and leading to both the putative $[(z_4 + H)^+ + (c_1 - H)^\bullet]$ and observed $[(y_1 + H)^+ + (b_4 - H)^\bullet]$ dissociation products were investigated following several pathways that were combined with proton migrations to form the $(c_1 - H)^\bullet$ radical as the more stable amide tautomer. The radical transfer was presumed to involve one of the C_α-hydrogens in the c_1 and b_4 fragments. The H

dx.doi.org/10.1021/jp411100c | J. Phys. Chem. A 2014, 118, 308−324

atom transfer reactions showed TS energies of 69−105 kJ mol^{-1}, which was in the same range as reported recently by Bythell for glycine cation-radical oligomers.[68] The pertinent energies and structures of intermediates and transitions states, as well as a detailed description of the reaction pathways, are given in the Supporting Information (Scheme S3 and S4).

DISCUSSION

The computational analysis of peptide cation-radical structures and reactions revealed some interesting features. Electron attachment to the most stable dication **1a**$^{2+}$ proceeded to the zwitterionic cation radical **1a**$^{+\bullet}$ as a local energy minimum on the potential energy surface of the ground electronic state. In contrast, electron attachment that was steered to the other amide groups in **1a**$^{2+}$, **1c**$^{2+}$, and **1i**$^{2+}$ resulted in proton migrations forming aminoketyl radicals **2a**$^{+\bullet}$−**4**$^{+\bullet}$.

Cation radical **1a**$^{+\bullet}$ was only marginally stable with respect to an exothermic proton migration, quenching the amide anion-radical and forming the aminoketyl radical **6**$^{+\bullet}$. These results indicate that amide anion-radicals, which have the electronic structure of amide π^* states, have intrinsic basicities that exceed those of the Lys and *N*-terminal amino groups. The present results are consistent with the Utah-Washington model of ExD which posits that amide π^* states produced by electron attachment are superbases that undergo exothermic proton migrations that convert them to aminoketyl radical intermediates.[11,14]

The distribution of amide π^* states is related to the properties of the electronic states accessible by electron attachment to the peptide dication. However, this relationship is not straightforward. The low electronic states of **1a**$^{+\bullet}$(vert), **1c**$^{+\bullet}$(vert), and **1i**$^{+\bullet}$(vert) were calculated to consist of combinations of ammonium 3s and 3p Rydberg and amide and carboxyl π^* orbitals that were delocalized over the peptide framework. This representation was generally independent of the TD-DFT method (B3LYP or M06-2X) although the wave functions representing the particular states differed for these DFT methods. The development of the virtual states into local energy minima on the potential energy surfaces of the ground and excited electronic states of the cation radicals depends on the state vibronic coupling that can be adequately described by time-dependent quantum dynamics.[25] A detailed analysis of excited-state dynamics would be a daunting task for a system of the GLGGK size. An interesting feature of gradient-based methods that converged to the ground electronic states was that they avoided the formation of Leu amide π^* states that would collapse to aminoketyl radical **3**$^{+\bullet}$. This effect was understandable in conformer **1a**$^{+\bullet}$(vert) where the Leu amide was not hydrogen bonded to the charged ammonium groups, so an intermediate Leu π^* amide state was presumed to be insufficiently stabilized by Coulomb effects. However, a similar avoidance of Leu amide reduction was also observed for conformers **1c**$^{+\bullet}$(vert) and **1i**$^{+\bullet}$(vert) where the Leu amide had strong hydrogen bonds to the Lys ammonium. To explain this effect would require a dynamics study that would include the vibrational motion of the amide atoms along the trajectory on the developing potential energy surface.

A novel feature revealed by the present study is the facile formation of structures **9**$^{+\bullet}$ and **10**$^{+\bullet}$ that are protonated at the amide nitrogen. These indicate that the amide π^* states produced by electron attachment can isomerize by N-protonation in addition to the previously considered O-protonation. Intermediates of the **9**$^{+\bullet}$ and **10**$^{+\bullet}$ type represent the missing link to backbone cleavages forming *y* type fragment ions via energetically plausible pathways. In the particular case of the GLGGK peptide, the formation of the y_1^+ and $b_4^{\bullet}$ fragments was disfavored by the high energy of the neutral radical.

Attempts to isomerize **1a**$^{+\bullet}$ by proton migration from a proximate neutral Gly_3 amide group led to a dynamically unstable intermediate (**5**$^{+\bullet}$) that was expected to isomerize back to **1a**$^{+\bullet}$. This result is consistent with the previous analysis of a similar isomerization in (AAVAR + 2H)$^{+\bullet}$,[65] indicating that intermediates like **5**$^{+\bullet}$ are unlikely to play a role in backbone dissociations. This casts further doubt on the "nonlocal" mechanism of ECD[5] (for a more detailed discussion see ref 14).

The backbone N−C_α cleavages can be considered to originate from radical intermediates such as amide zwitterions or aminoketyl radicals. The aminoketyl intermediates are unlikely to interconvert by hydrogen atom transfers in competition with N−C_α bond cleavages. This stems from the calculated relative energies that place **6**$^{+\bullet}$ as the global aminoketyl radical minimum that should dominate at equilibrium. However, dissociations starting from **6**$^{+\bullet}$ prefer loss of ammonia (vide supra), which would competitively suppress backbone cleavages, in contradiction with the experimental data.

Structures **1a**$^{+\bullet}$ and **6**$^{+\bullet}$ are reactive intermediates for the competitive loss of ammonia and cleavage of the Gly_1-Leu N−C_α bond that collectively account for 33% of fragmentations. Cleavage of the Leu-Gly_3 N−C_α bond can proceed from **3**$^{+\bullet}$ by a standard aminoketyl mechanism or from **2a**$^{+\bullet}$ by an enol-type cleavage through **TS8**. These dissociations are collectively abundant, leading to $z_3^{+\bullet}$ fragment ions that account for 10% of ETD fragments. Interestingly, the enol cleavage in **2a**$^{+\bullet}$ is reversible and therefore kinetically disfavored due to the high energy of the incipient $(z_3 + c_2)^{+\bullet}$ complex. Hence, most of $z_3^{+\bullet}$ fragment ions is presumed to arise from **3**$^{+\bullet}$ by a standard aminoketyl mechanism.

Cleavage of the Gly_3-Gly_4 N−C_α bond can proceed from the Gly_3 aminoketyl radicals **2a**$^{+\bullet}$, **2b**$^{+\bullet}$, and **7**$^{+\bullet}$, which are readily accessible by electron attachment followed by a collapse to the ground electronic states of the pertinent aminoketyl radicals. In contrast, the Gly_3-Gly_4 bond cleavage is less abundant upon ETD, leading to the formation of the minor $z_3^{+\bullet}$ fragment ions at only 3%. We note that structures **2a**$^{+\bullet}$ and **2b**$^{+\bullet}$ are chiefly accessible from very minor precursor ion conformers and thus may not appreciably contribute to the formation of $z_3^{+\bullet}$ fragment ions. Finally, cleavage of the Gly_4-Lys N−C_α bond can proceed from the Gly_4 aminoketyl radical **4**$^{+\bullet}$ via a standard mechanism, or from **8**$^{+\bullet}$−**10**$^{+\bullet}$ via the novel mechanism depicted by **TS5**. This dissociation must be accompanied by a proton transfer in the very stable $(z_1 + c_4)^{+\bullet}$ complex **13**$^{+\bullet}$ to proceed to the formation of the abundant c_4^+ fragment ion (11%) rather than the $z_1^{+\bullet}$, which is barely detectable upon ETD.

CONCLUSIONS

On the basis of the analysis of the dissociation pathways and TS energies in GLGGK cation-radicals, we arrive at the conclusion that the formation of the backbone and other fragments is not completely governed by kinetically competitive reactions. Rather, the reaction course is set by the structure of the reactive intermediate, a zwitterion or an aminoketyl radical, accessed by electron transfer. From this point of view, the individual TS energies affect the kinetics of only those

dissociations that originate from a common reactant. In contrast, a large part of the dissociation branching occur at the stage where the reactive intermediates are formed by vibronic transitions from the electronic states developing in the course of electron transfer. These conclusions are in line with previous studies of peptide cation-radical dissociations where fragment branching ratios calculated on the basis of competitive kinetic models did not reflect experimental values from ETD mass spectra.[8,15,25]

■ ASSOCIATED CONTENT

Supporting Information

Complete refs 15, 36, and 52. Figures S1–S6 (plots for the pseudo-first order peptide ion–fluoranthene anion reactions, ETD-CID-MS^3 spectrum, time dependence profiles, M06-2X/6-31+G(d,p) optimized structures, molecular orbitals) and Schemes S1–S4 (enol-side bond dissociations, hydrogen atom migrations) and their related text. This material is available free of charge via the Internet at http://pubs.acs.org.

■ AUTHOR INFORMATION

Present Address

[†]Institute of Organic Chemistry and Biochemistry, Academy of Sciences of the Czech Republic, 166 10 Prague, Czech Republic.

Notes

The authors declare no competing financial interest.

■ ACKNOWLEDGMENTS

Support of this work by the NSF Chemistry Division (Grant CHE-1055132 to F.T.) is gratefully acknowledged. K.J.L. thanks the ARCS foundation for financial support. The authors thank Drs. Rob Moritz of the Seattle Institute for Systems Biology and Xiaoyun Fu of the Puget Sound Blood Center for kindly providing access to the Thermo-Fisher Orbitrap ETD Elite and Velos instruments, respectively, and Dr. Jan Urban for valuable advice with peptide syntheses.

■ REFERENCES

(1) Zubarev, R. A.; Kelleher, N. L.; McLafferty, F. W. Electron Capture Dissociation of Multiply Charged Protein Cations. A Nonergodic Process. *J. Am. Chem. Soc.* **1998**, *120*, 3265–3266.

(2) Syka, J. E. P.; Coon, J. J.; Schroeder, M. J.; Shabanowitz, J.; Hunt, D. F. Peptide and Protein Sequence Analysis by Electron Transfer Dissociation Mass Spectrometry. *Proc. Natl. Acad. Sci. U. S. A.* **2004**, *101*, 9528–9533.

(3) Coon, J. J. Collisions or Electrons? Protein Sequence Analysis in the 21st Century. *Anal. Chem.* **2009**, *81*, 3208–3215.

(4) Mihalca, R.; Kleinnijenhuis, A. J.; McDonnell, L. A.; Heck, A. J. R.; Heeren, R. M. A. Electron Capture Dissociation at Low Temperatures Reveals Selective Dissociations. *J. Am. Soc. Mass Spectrom.* **2004**, *15*, 1869–1873.

(5) Patriksson, A.; Adams, C.; Kjeldsen, F.; Raber, J.; van der Spoel, D.; Zubarev, R. A. Prediction of N-Cα Bond Cleavage Frequencies in Electron Capture Dissociation of Trp-cage Dications by Force-Field Molecular Dynamics Simulations. *Int. J. Mass Spectrom.* **2006**, *248*, 124–135.

(6) Tureček, F.; Chen, X.; Hao, C. Where Does the Electron Go? Electron Distribution and Reactivity of Peptide Cation-Radicals Formed by Electron Transfer in the Gas Phase. *J. Am. Chem. Soc.* **2008**, *130*, 8818–8833.

(7) Ben Hamidane, H.; He, H.; Tsybin, O. Y.; Emmett, M. R.; Hendrickson, C. L.; Marshall, A. G.; Tsybin, Y. O. Periodic Sequence Distribution of Product Ion Abundances in Electron Capture Dissociation of Amphipathic Peptides and Proteins. *J. Am. Soc. Mass Spectrom.* **2009**, *20*, 1182–1192.

(8) Moss, C. L.; Chung, T. W.; Čeřovský, V.; Tureček, F. Electron Transfer Dissociation of a Melectin Peptide: Correlating the Precursor Ion Structure with Peptide Backbone Dissociations. *Collect. Czech. Chem. Commun.* **2011**, *76*, 295–309.

(9) Prell, J. S.; O'Brien, J. T.; Holm, A. I. S.; Leib, R. D.; Donald, W. A.; Williams, E. R. Electron Capture by a Hydrated Gaseous Peptide: Effects of Water on Fragmentation and Molecular Survival. *J. Am. Chem. Soc.* **2008**, *130*, 12680–12689.

(10) Chung, T. W.; Tureček, F. Proper and Improper Aminoketyl Radicals in Electron-Based Peptide Dissociations. *Int. J. Mass Spectrom.* **2011**, *301*, 55–61.

(11) Syrstad, E. A.; Tureček, F. Toward a General Mechanism of Electron-Capture Dissociation. *J. Am. Soc. Mass Spectrom.* **2005**, *16*, 208–224.

(12) Skurski, P.; Sobczyk, M.; Jakowski, J.; Simons, J. Possible Mechanisms for Protecting NCα Bonds in Helical Peptides from Electron-Capture (or Transfer) Dissociation. *Int. J. Mass Spectrom.* **2007**, *265*, 197–212.

(13) Neff, D.; Sobczyk, M.; Simons, J. Through-Space and Through-Bond Electron Transfer within Positively Charged Peptides in the Gas Phase. *Int. J. Mass Spectrom.* **2008**, *276*, 91–101.

(14) Tureček, F.; Julian, R. R. Peptide Radicals and Cation-Radicals in the Gas Phase. *Chem. Rev.* **2013**, *113*, 6691–6733.

(15) Tureček, F.; Chung, T. W.; Moss, C. L.; Wyer, J. A.; Ehlerding, A.; Holm, A. I. S.; Zettergren, H.; Nielsen, S. B.; Hvelplund, P.; Chamot-Rooke, J.; et al. The Histidine Effect. Electron Transfer and Capture Cause Different Dissociations and Rearrangements of Histidine Peptide Cation-Radicals. *J. Am. Chem. Soc.* **2010**, *132*, 10728–10740.

(16) Moss, C. L.; Chung, T. W.; Wyer, J. A.; Nielsen, S. B.; Hvelplund, P.; Tureček, F. Dipole-Guided Electron Capture Causes Abnormal Dissociations of Phosphorylated Pentapeptides. *J. Am. Soc. Mass Spectrom.* **2011**, *22*, 731–751.

(17) Swierszcz, I.; Skurski, P.; Simons, J. Dipole and Coulomb Forces in Electron Capture Dissociation and Electron Transfer Dissociation Mass Spectroscopy. *J. Phys. Chem. A* **2012**, *116*, 1828–1837.

(18) Kjeldsen, F.; Haselmann, K. F.; Budnik, B. A.; Jensen, F.; Zubarev, R. A. Dissociative Capture of Hot (3–13 eV) Electrons by Polypeptide Polycations: An Efficient Process Accompanied by Secondary Fragmentation. *Chem. Phys. Lett.* **2002**, *356*, 201–206.

(19) Fung, Y. M. E.; Chan, T.-W. D. Experimental and Theoretical Investigations of the Loss of Amino Acid Side Chains in Electron Capture Dissociation of Model Peptides. *J. Am. Soc. Mass Spectrom.* **2005**, *16*, 1523–1535.

(20) Faelth, M.; Savitski, M. M.; Nielsen, M. L.; Kjeldsen, F.; Andren, P. E.; Zubarev, R. A. Analytical Utility of Small Neutral Losses from Reduced Species in Electron Capture Dissociation Studied Using SwedECD Database. *Anal. Chem.* **2008**, *80*, 8089–8094.

(21) Liu, J.; Liang, X.; McLuckey, S. A. On the Value of Knowing a z.bul. Ion for What It Is. *J. Proteome Res.* **2008**, *7*, 130–137.

(22) Han, H.; Xia, Y.; McLuckey, S. A. Ion Trap Collisional Activation of c and z.bul. Ions Formed via Gas-Phase Ion/Ion Electron-Transfer Dissociation. *J. Proteome Res.* **2007**, *6*, 3062–3069.

(23) Chung, T. W.; Tureček, F. Backbone and Side-Chain Specific Dissociations of z Ions from Non-Tryptic Peptides. *J. Am. Soc. Mass Spectrom.* **2010**, *21*, 1279–1295.

(24) Xia, Q.; Lee, M. V.; Rose, C. M.; Marsh, A. J.; Hubler, S. L.; Wenger, C. D.; Coon, J. J. Characterization and Diagnostic Value of Amino Acid Side Chain Neutral Losses Following Electron-Transfer Dissociation. *J. Am. Soc. Mass Spectrom.* **2011**, *22*, 255–264.

(25) Moss, C. L.; Liang, W.; Li, X.; Tureček, F. The Early Life of a Peptide Cation Radical. Ground and Excited-State Trajectories of Electron-Based Peptide Dissociations During the First 330 fs. *J. Am. Soc. Mass Spectrom.* **2012**, *23*, 446–459.

(26) Coste, J.; LeNguyen, D.; Castro, B. PyBOP®: A New Peptide Coupling Reagent Devoid of Toxic By-product. *Tetrahedron Lett.* **1990**, *31* (2), 205–208.

(27) Marek, A.; Pepin, R.; Peng, B.; Laszlo, K. J.; Bush, M. F.; Tureček, F. Electron Transfer Dissociation of Photolabeled Peptides. Backbone Cleavages Compete with Diazirine Ring Rearrangements. *J. Am. Soc. Mass Spectrom.* **2013**, *24*, 1641−1653.
(28) Pringle, S. D.; Giles, K.; Wildgoose, J. L.; Williams, J. P.; Slade, S. E.; Thalassinos, K.; Bateman, R. H.; Bowers, M. T.; Scrivens, J. H. An Investigation of the Mobility Separation of Some Peptide and Protein Ions Using a New Hybrid Quadrupole/Travelling Wave IMS/oa-ToF Instrument. *Int. J. Mass Spectrom.* **2007**, *261*, 1−10.
(29) Giles, K.; Williams, J. P.; Campuzano, I. Enhancements in Travelling Wave Ion Mobility Resolution. *Rapid Commun. Mass Spectrom.* **2011**, *25*, 1559−1566.
(30) Williams, J. P.; Brown, J. M.; Campuzano, I.; Sadler, P. J. Identifying Drug Metallation Sites on Peptides Using Electron Transfer Dissociation (ETD), Collision Induced Dissociation (CID) and Ion Mobility-Mass Spectrometry (IM-MS). *Chem. Commun.* **2010**, *46*, 5458−5460.
(31) Bush, M. F.; Hall, Z.; Giles, K.; Hoyes, J.; Robinson, C. V.; Ruotolo, B. T. Collision Cross Sections of Proteins and Their Complexes: A Calibration Framework and Database for Gas-Phase Structural Biology. *Anal. Chem.* **2010**, *82*, 9557−9565.
(32) Allen, S. J.; Marionni, S. T.; Giles, K.; Gilbert, T.; Bush, M. F. Design and Characterization of a New Ion Mobility Cell for Protein Complexes. Presented at the 60th American Society for Mass Spectrometry Conference, Vancouver, BC, 2012.
(33) Mason, E. A.; McDaniel, E. W. *Transport Properties of Ions in Gases*; Wiley: New York, 1998; pp 149, 408.
(34) Moss, C. L.; Chamot-Rooke, J.; Brown, J.; Campuzano, I.; Richardson, K.; Williams, J.; Bush, M.; Bythell, B.; Paizs, B.; Turecek, F. Assigning Structures to Gas-Phase Peptide Cations and Cation-Radicals. An Infrared Multiphoton Dissociation, Ion Mobility, Electron Transfer and Computational Study of a Histidine Peptide Ion. *J. Phys Chem. B* **2012**, *106*, 3445−3456.
(35) Phillips, J. C; Braun, R.; Wang, W.; Gumbart, J.; Tajkhorshid, E.; Villa, E.; Chipot, C.; Skeel, R. D.; Kale, L.; Schulten, K. Scalable Molecular Dynamics with NAMD. *J. Comput. Chem.* **2005**, *26*, 1781−1802.
(36) MacKerell, A. D., Jr.; Bashford, D.; Bellott, M.; Dunbrack, R. L., Jr.; Evanseck, J. D.; Field, M. J.; Fischer, S.; Gao, J.; Guo, H.; Ha, S.; et al. All-Atom Empirical Potential for Molecular Modeling and Dynamics Studies of Proteins. *J. Phys. Chem. B* **1998**, *102*, 3586−3616.
(37) Sugita, Y.; Okamoto, Y. Replica-Exchange Molecular Dynamics Method for Protein Folding. *Chem. Phys. Lett.* **1999**, *314*, 141−151.
(38) Stewart, J. J. P. Optimization of Parameters for Semiempirical Methods. V. Modification of NDDO Approximations and Application to 70 Elements. *J. Mol. Model.* **2007**, *13*, 1173−1213.
(39) Becke, A. D. New Mixing of Hartree-Fock and Local Density-Functional Theories. *J. Chem. Phys.* **1993**, *98*, 1372−1377.
(40) Becke, A. D. Density Functional Thermochemistry. III. The Role of Exact Exchange. *J. Chem. Phys.* **1993**, *98*, 5648−5652.
(41) Zhao, Y.; Truhlar, D. G. The M06 Suite of Density Functionals for Main Group Thermochemistry, Thermochemical Kinetics, Noncovalent Interactions, Excited States, and Transition Elements: Two New Functionals and Systematic Testing of Four M06-class Functionals and 12 Other Functionals. *Theor. Chem. Acc.* **2008**, *120*, 215−241.
(42) McClurg, R. B.; Flagan, R. C.; Goddard, W. A., III. The Hindered Rotor Density-of-States Interpolation Function. *J. Chem. Phys.* **1997**, *106*, 6675−6680.
(43) Ayala, P. Y.; Schlegel, H. B. Identification and Treatment of Internal Rotation in Normal Mode Vibrational Analysis. *J. Chem. Phys.* **1998**, *108*, 2314−2325.
(44) Møller, C.; Plesset, M. S. A Note on an Approximation Treatment for Many-Electron Systems. *Phys. Rev.* **1934**, *46*, 618−622.
(45) Fukui, K. The Path of Chemical Reactions - the IRC Approach. *Acc. Chem. Res.* **1981**, *14*, 363−368.
(46) Hratchian, H. P.; Schlegel, H. B. Accurate Reaction Paths Using a Hessian Based Predictor-Corrector Integrator. *J. Chem. Phys.* **2004**, *120*, 9918−9924.
(47) Schlegel, H. B. Potential Energy Curves Using Unrestricted Moller-Plesset Perturbation Theory with Spin Annihilation. *J. Chem. Phys.* **1986**, *84*, 4530−4534.
(48) Mayer, I. Spin-Projected UHF Method. IV. Comparison of Potential Curves Given by Different One-Electron Methods. *Adv. Quantum Chem.* **1980**, *12*, 189−262.
(49) Tureček, F. Proton Affinity of Dimethyl Sulfoxide and Relative Stabilities of C_2H_6OS Molecules and $C_2H_7OS^+$ Ions. A Comparative G2(MP2) ab Initio and Density Functional Theory Study. *J. Phys. Chem. A* **1998**, *102*, 4703−4713.
(50) Rablen, P. R. Is the Acetate Anion Stabilized by Resonance or Electrostatics? A Systematic Structural Comparison. *J. Am. Chem. Soc.* **2000**, *122*, 357−368.
(51) Furche, F.; Ahlrichs, A. Adiabatic Time-Dependent Density Functional Methods for Excited State Properties. *J. Chem. Phys.* **2002**, *117*, 7433−7447.
(52) Frisch, M. J.; Trucks, G. W.; Schlegel, H. B.; Scuseria, G. E.; Robb, M. A.; Cheeseman, J. R.; Scalmani, G.; Barone, V.; Mennucci, B.; Petersson, G. A.; et al. *Gaussian 09*, Revision A.02; Gaussian, Inc.: Wallingford, CT, 2009.
(53) Reed, A. E.; Weinstock, R. B.; Weinhold, F. Natural Population Analysis. *J. Chem. Phys.* **1985**, *83*, 735−746.
(54) Gilbert, R. G.; Smith, S. C. *Theory of Unimolecular and Recombination Reactions*; Blackwell Scientific Publications: Oxford, U.K., 1990; pp 52−132.
(55) Zhu, L.; Hase, W. L. *Quantum Chemistry Program Exchange*; Indiana University: Bloomington, 1994.
(56) Frank, A. J.; Sadílek, M.; Ferrier, J. G.; Tureček, F. Sulfur Oxyacids and Radicals in the Gas Phase. A Variable-Time Neutralization-Photoexcitation-Reionization Mass Spectrometric and Ab Initio/RRKM Study. *J. Am. Chem. Soc.* **1997**, *119*, 12343−12353.
(57) Gellene, G. I.; Cleary, D. A.; Porter, R. F. Stability of the Ammonium and Methylammonium Radicals from Neutralized Ion-Beam Spectroscopy. *J. Chem. Phys.* **1982**, *77*, 3471−3477.
(58) Gellene, G. I.; Porter, R. F. Neutralized Ion-Beam Spectroscopy. *Acc. Chem. Res.* **1983**, *16*, 200−209.
(59) Shaffer, S. A.; Tureček, F. Hydrogentrimethylammonium. A Marginally Stable Hypervalent Radical. *J. Am. Chem. Soc.* **1994**, *116*, 8647−8653.
(60) Nguyen, V. Q.; Sadílek, M.; Frank, A. J.; Ferrier, J. G.; Tureček, F. Metastable States of Dimethylammonium Radical. *J. Phys. Chem. A* **1997**, *101*, 3789−3799.
(61) Yao, C.; Tureček, F. Hypervalent Ammonium Radicals. Competitive N-C and N-H Bond Dissociations in Methylammonium and Ethylammonium. *Phys. Chem. Chem. Phys.* **2005**, *7*, 912−920.
(62) Holm, A. I. S.; Hvelplund, P.; Kadhane, U.; Larsen, M. K.; Liu, B.; Nielsen, S. B.; Panja, S.; Pedersen, J. M.; Skrydstrup, T.; Stochkel, K.; Williams, E. R.; Worm, E. S. On the Mechanism of Electron-Capture-Induced Dissociation of Peptide Dications from ^{15}N-labeling and Crown-Ether Complexation. *J. Phys. Chem. A* **2007**, *111*, 9641−9643.
(63) von Helden, G.; Hsu, M. T.; Gotts, N.; Bowers, M. T. Carbon Cluster Cations with up to 84 Atoms: Structures, Formation Mechanism, and Reactivity. *J. Phys. Chem.* **1993**, *97*, 8182−8192.
(64) Mesleh, M. F.; Hunter, J. M.; Shvartsburg, A. A.; Schatz, G. C.; Jarrold, M. F. Structural Information from Ion Mobility Measurements: Effects of the Long-Range Potential. *J. Phys. Chem.* **1996**, *100*, 16082−16086.
(65) Tureček, F.; Moss, C. L.; Chung, T. W. Correlating ETD Fragment Ion Intensities with Peptide Ion Conformational and Electronic Structure. *Int. J. Mass Spectrom.* **2012**, *330*−*332*, 207−219.
(66) Tureček, F.; Panja, S.; Wyer, J. A.; Ehlerding, A.; Zettergen, H.; Nielsen, S. B.; Hvelplund, P.; Bythell, B.; Paizs, B. Carboxyl-Catalyzed Prototropic Rearrangements in Histidine Peptide Radicals upon Electron Transfer. Effects of Peptide Sequence and Conformation. *J. Am. Chem. Soc.* **2009**, *131*, 16472−16487.
(67) Wodrich, M. D.; Zhurov, K. O.; Vorobyev, A.; Ben Hamidane, H.; Corminboeuf, C.; Tsybin, Y. O. Heterolytic N-Cα Bond Cleavage

in Electron Capture and Transfer Dissociation of Peptide Cations. *J. Phys. Chem. B* **2012**, *116*, 10807−10815.
(68) Bythell, B. J. To Jump or Not To Jump? Cα Hydrogen Atom Transfer in Post-Cleavage Radical-Cation Complexes. *J. Phys. Chem. A* **2013**, *117*, 1189−1196.